Graphene Oxide-Based Nanocomposites for Environmental Protection

By

Vania Sayyab

Registration No: 00000401682

Department of Materials Engineering

School of Chemical and Materials Engineering

National University of Sciences & Technology (NUST)

Islamabad, Pakistan

(2024)

Graphene Oxide-Based Nanocomposites for Environmental Protection

By

Vania Sayyab

Registration No: 00000401682

A thesis submitted to the National University of Sciences and Technology, Islamabad,

in partial fulfillment of the requirements for the degree of

Master of Science in
Nanoscience & Engineering

Supervisor: Dr. Zakir Hussain

Co Supervisor: Dr. Hamza Qayyum

School of Chemical and Materials Engineering

National University of Sciences & Technology (NUST)

Islamabad, Pakistan

(2024)

THESIS ACCEPTANCE CERTIFICATE

Certified that final copy of MS Thesis entitled "**Graphene Oxide-based Nanocomposites for Environmental Protection**" written by Ms **Vania Sayyab** (Registration No 00000401682), of School of Chemical & Materials Engineering (SCME) has been vetted by undersigned, found complete in all respects as per NUST Statues/Regulations, is free of plagiarism, errors, and mistakes and is accepted as partial fulfillment for award of MS degree. It is further certified that necessary amendments as pointed out by GEC members of the scholar have also been incorporated in the said Thesis.

Signature: _____

Name of Supervisor: **Dr Zakir Hussain**

Date: 2/12/2024

Signature (HOD): _____

Date: 03-12-24

Signature (Dean/Principal): _____

Date: 4/12/24

National University of Sciences &Technology (NUST)

FORM TH-4

MASTER'S THESIS WORK

We hereby recommend that the dissertation prepared under our supervision by

Regn No & Name: **00000401682 Vania Sayyab**

Title: **Graphene Oxide-based Nanocomposites for Environmental Protection.**

Presented on: **30 Oct 2024** at: **1500 hrs in SCME Seminar Hall**

Be accepted in partial fulfillment of the requirements for the award of Masters of Science degree in **Nanoscience & Engineering.**

Guidance & Examination Committee Members

Name: **Dr M. Bilal Khan Niazi** Signature:

Name: **Dr Usman Liaqat** Signature:

Name: **Dr Hamza Qayyum** (Co-Supervisor) Signature:

Supervisor's Name: **Dr Zakir Hussain** Signature:

Dated: 31.10.2024

Head of Department

04-11-24
Date

COUNTERSIGNED

Date 04-04-2024

4/11/24
Dean/Principal

School of Chemical &Materials Engineering (SCME)

AUTHOR'S DECLARATION

I Vania Sayyab hereby state that my MS thesis titled "Graphene Oxide-Based Nanocomposites for Environmental Protection" is my own work and has not been submitted previously by me for taking any degree from National University of Sciences and Technology, Islamabad or anywhere else in the country/ world.

At any time if my statement is found to be incorrect even after I graduate, the university has the right to withdraw my MS degree.

Name of Student: Vania Sayyab

Date: _____

PLAGIARISM UNDERTAKING

I solemnly declare that research work presented in the thesis titled "Graphene Oxide-Based Nanocomposite for Environmental Protection" is solely my research work with no significant contribution from any other person. Small contribution/ help wherever taken has been duly acknowledged and that complete thesis has been written by me.

I understand the zero tolerance policy of the HEC and National University of Sciences and Technology (NUST), Islamabad towards plagiarism. Therefore, I as an author of the above titled thesis declare that no portion of my thesis has been plagiarized and any material used as reference is properly referred/cited.

I undertake that if I am found guilty of any formal plagiarism in the above titled thesis even after award of MS degree, the University reserves the rights to withdraw/revoke my MS degree and that HEC and NUST, Islamabad has the right to publish my name on the HEC/University website on which names of students are placed who submitted plagiarized thesis.

Student Signature: _____

Name: Vania Sayyab

DEDICATION

To my loved ones who constantly motivated me to never give up and survived my project rants.

ACKNOWLEDGEMENTS

First and foremost, I would like to express my sincere gratitude to my supervisor, **Dr. Zakir Hussain** and co-supervisor **Dr. Hamza Qayyum** for their patience, encouragement, and endless guidance without which the completion of this work wouldn't be possible. Their mentorship has shaped the direction of my work, and I am forever grateful for the opportunities they provided for my academic growth. I would also like to extent my sincere gratitude to my committee members, **Dr. Usman Liaqat**, and **Dr. Muhammad Bilal Khan Niazi.**

I cannot express my gratitude and appreciation for the love and support that my parents, who have dedicated towards enabling me to pursue my dreams in any path of my choosing. Without their tireless efforts, I would never be where I am now. The same appreciation extends to the rest of my family, especially to my sister **Shumaila Sayyab**. I must also acknowledge my friends whose unwavering love and constant attention, support and encouragement have helped me to overcome the difficult feelings and kept my motivation levels high whenever I was overwhelmed.

.

TABLE OF CONTENTSs

SSACKNOWLEDGEMENTS **VIII**

TABLE OF CONTENTSS **IX**

LIST OF TABLES **XI**

LIST OF FIGURES **XII**

LIST OF SYMBOLS, ABBREVIATIONS AND ACRONYMS **XIII**

ABSTRACT **XV**

CHAPTER 1: INTRODUCTION **1**

CHAPTER 2: LITERATURE REVIEW **5**
2.1 Introduction **5**
2.2 Graphene Oxide **6**
2.2.1 Synthesis of GO 6
2.2.2 Applications of GO 8
2.3 Silver Nanoparticles **8**
2.3.1 Synthesis Methods 9
2.4 Pulsed Laser Ablation in Liquid **10**
2.5 Challenges and Limitations **12**
2.6 Graphene Oxide-Silver (GO-Ag) Nanocomposites **13**
2.6.1 Synthesis Methods for GO-Ag Composites 13
2.6.2 Applications of GO-Ag Composites 14

CHAPTER 3: MATERIALS AND METHOD **17**
3.1 Synthesis and formation **17**
3.1.1 Graphene Oxide 17
3.1.2 Graphene Oxide-Silver Nanocomposites 18
3.2 Characterization of Materials **21**
3.2.1 Fourier Transform Infrared Spectroscopy (FTIR) 21
3.2.2 Ultraviolet-Visible spectroscopy (UV-Vis) 22
3.2.3 X-ray Diffraction (XRD) 22
3.2.4 Scanning Electron Microscopy (SEM) and Energy Dispersive Spectroscopy (EDS) 22
3.2.5 Raman Spectroscopy 22
3.2.6 Zeta potential 23
3.3 Application-based testing **23**
3.3.1 Antibacterial Assay 23
3.3.2 Surface Enhanced Raman Spectroscopy (SERS) 27

CHAPTER 4: RESULTS AND DISCUSSION **29**

4.1 Characterization of Materials 29
4.1.1 FTIR of GO 29
4.1.2 UV-Vis of GO, GO-AgMC, and GO-AgNS 30
4.1.3 XRD of GO, GO-AgMC, and GO-AgNS 31
4.1.4 SEM of GO, GO-AgMC, and GO-AgNS 33
4.1.5 Raman of GO, GO-AgMC, and GO-AgNS 36
4.1.6 Zeta Potential 38
4.2 Structure turnability/ parameter optimization of cubic composite 39
4.3 ANTIBACTERIAL 41
4.3.1 GO pH-dependant antibacterial 41
4.3.2 Composites' shape-dependent antibacterial 44
4.4 SURFACE ENHANCED RAMAN SPECTROSCOPY (SERS) 46

CONCLUSIONS AND FUTURE PROSPECTIVE 48

REFERENCES 50

LIST OF TABLES

Table 3-1: Laser parameters for the synthesis of GO-Ag composites 21
Table 4-1: Zeta potential of GO during prolong sonication. 38
Table 4-2: Zeta potential of colloidal synthesised materials. 38

LIST OF FIGURES

Figure 1.1: Types of environmental contaminants present in air, soil and water. 1
Figure 1.2: GO-based composites and their environmental applications. 2
Figure 1.3: The mode of action of AgNPs on microbials. 3
Figure 2.1: 0D, 1D and 3D carbon material formed from 2D graphene. 5
Figure 2.2: Schematic of GO sheet. 6
Figure 2.3 Nanomaterial synthesis approaches and techniques. 10
Figure 2.4: Schematics diagram of basic PLAL mechanisms. 11
Figure 2.5: Applications of multifunction GO-Ag composites. 15
Figure 3.1: Schematic diagram of Improved Hummer's Method. 18
Figure 3.2: Sonication of GO solution in ice/water bath. 19
Figure 3.3: Schematic diagrams of the PLAL experimental setup. 20
Figure 3.4: Plate count method for antibacterial assay. 25
Figure 3.5: 96-well plate method for antibacterial assay. 26
Figure 3.6: Schematic of SERS sample preparation. 28
Figure 4.1: FTIR spectra of GO. 29
Figure 4.2: (a) UV-Vis spectrum (b) Bandgap of GO, GO-AgMC and GO-AgNS. 30
Figure 4.3: XRD spectrum of GO, GO-AgMC and GO-AgNS. 32
Figure 4.4: SEM images of (a) GO, (b) GO-AgMC, (c) GO-AgNS, (d) GO-AgMC after 3 months. 34
Figure 4.5: EDS of GO-AgMC. 35
Figure 4.6: Elemental mapping of GO-AgMC. 36
Figure 4.7: Raman spectrum of GO, GO-AgMC and GO-AgNS. 37
Figure 4.8: SEM image of GO-AgMC at varying parameters; (a) 5 mins, (b) 10 mins and 140 mJ, (c) 12 mins, (d) 15 mins, (e) 106 mJ, and (f) 172 mJ. 39
Figure 4.9: UV-Vis spectrum of GO-AgMC at (A) varying time and (B) varying energy. 40
Figure 4.10: Antibacterial activity of GO produced at pH 3, 4 and 5.5 against *E. coli*. 42
Figure 4.11: Antibacterial activity of GO at pH 3, 4, 5.5, 7 and 8 against *E. coli*. 43
Figure 4.12: Antibacterial activity of synthesized material and the images of the 96 well plate against (A),(B) E.coli and (C), (D) S. aureus, respectively. 44
Figure 4.13: SERS of methylene blue (MB) with GO, AgNPs, and GO-AgMC. 46

LIST OF SYMBOLS, ABBREVIATIONS AND ACRONYMS

Ag^+	Silver ions
AgNPs	Silver Nanoparticles
CuONPs	Copper Oxide Nanoparticles
CVD	Chemical Vapor Deposition
DI	Deionized (Water)
EDS	Energy dispersive X-ray Spectroscopy
FTIR	Fourier Transform Infrared Spectroscopy
FWHM	Full Wave Half Maximum
GO	Graphene Oxide
GO-Ag	Graphene Oxide-Silver
GO-Ag	Graphene Oxide-Silver Nano Sphere
GO-AgMC	Graphene Oxide-Silver Micro Cube
H_2O_2	Hydrogen Peroxide
H_2SO_4	Sulfuric Acid
H_3PO_4	Phosphoric Acid
HNO_3	Nitric Acid
$KCLO_3$	Potassium Chlorate
$KMnO_4$	Potassium Permanganate
LB	Lysogeny Broth
LSPR	Localized Surface Plasmon Resonance
MB	Methylene Blue
$NaHCO_3$	Sodium Bicarbonate
$NaNO_3$	Sodium Nitrate

Nd-YAG	Neodymium-Doped Yttrium Aluminium Garnet
OD	Optical Density
PLAL	Pulsed Laser Ablation in Liquid
rGO	Reduced Graphene Oxide
ROS	Reactive Oxygen Species
SEM	Scanning Electron Microscopy
SERS	Surfaced Enhanced Raman Spectroscopy
SPR	Surface Plasmon Resonance
TSC	Trisodium Citrate
UV-Vis	Ultraviolet-Visible Spectroscopy
XRD	X-ray Diffraction

ABSTRACT

The exponentially increasing chemical pollutants and highly resistive pathogens have made it a necessity for the development of an innovative, multifunctional material. Graphene oxide (GO) and silver nanoparticles (AgNPs), both exhibit excellent antibacterial, sensing, and catalytical properties thereby being the ideal choice to investigate the integration of the nanomaterial into environmental applications. Various methods can be opted to synthesize GO-based nanocomposites however each technique has its benefits and drawbacks. Therefore, this thesis explores an improved Hummer's method and Pulsed Laser Ablation in Liquid (PLAL) for the fabrication of high-quality GO and surfactant-free graphene oxide-silver (GO-Ag) composites, respectively. In a simple and fast PLAL procedure, a pure silver target plate, immersed in fully dispersed GO solution, is ablated by an Nd-YAG nanosecond laser. Thereby forming a highly stable colloidal composite without the use of any chemical agents or harmful by-products. The laser parameters had been optimized to control the specific characteristics of the GO-Ag composite for enhancing the antibacterial and sensing properties. As such the ablation process was carried out with a 1064 nm laser for varying time and varying energy. After various trials, the optimal parameters were deduced as 140 mJ energy and 10 mins. Moreover, the synthesized materials were confirmed by multiple diagnostic techniques including FTIR, UV-Vis spectroscopy, SEM, EDS, Raman, Zeta potential analysis, and XRD. Thereby giving an insight into the chemical properties, structure, and morphology of the fabricated composites. Subsequently, the antibacterial activity and potential in SERS were evaluated. The results demonstrated that GO-Ag composites have superior antibacterial activity, SERS

capability, and stability compared to the individual components; GO and Ag. Additionally, the cubic shape GO-Ag micro-composite had better antibacterial performance than that of the spherical GO-Ag nanocomposite. Thus GO-Ag composite with optimized properties is a promising multifunctional material for environmental protection.

Keywords: graphene oxide, noble metal nanoparticles, pulsed laser ablation in liquid, antibacterial, surface-enhanced Raman spectroscopy

CHAPTER 1: INTRODUCTION

The worldwide human health crises are attributed to interconnected chemical pollutants and pathogens. These environmental contaminants are exponentially on the rise due to industrialization, urbanization, and the swift progress of the healthcare system. As illustrated in **Figure 1.1** they are incorporated in air, soil, and water in the form of heavy metals, plastics, dyes, and various disease-causing microbes, bacteria, viruses, etc. Chemically pollutants are conventionally treated through chemicals that have harmful byproducts, slow biological processes, or by expensive advance filtration systems [1], [2]. Whereas pathogenic remediation involves the use of various chemical reagents and water disinfection methods like UV treatment and chlorination. However, they generate byproducts that can be carcinogenic and involve expensive equipment with limited effectiveness. Furthermore, they lead to antimicrobial resistance with prolonged use and have limited specificity and efficiency [3], [4]. Thereby leading to more resilient infections. Consequently, a new environmentally friendly, innovative, and multifunctional material is required to address the growing chemical and environmental pollutants for the betterment of human life.

Figure 1.1: Types of environmental contaminants present in air, soil and water.

Various nanomaterials have been explored due to their extraordinary properties, to resolve these correlated issues. However, reaching a complete solution is still difficult. Graphene oxide (GO), a derivative of graphene, consists of a monolayer of sp^2 hybridized hexagonal carbon atoms and oxygen-containing functional groups. Due to its exceptional characteristics such as large surface area, mechanical strength, biocompatibility, great electrical conductivity, and excellent adsorption capabilities, it has gained significant recent attention in multiple applications [5]. Such as electronics, energy, and environmental remediation [6], [7].

Figure 1.2: GO-based composites and their environmental applications.

The functionality of GO increases the hydrophilicity and tunability of the material thereby making it the perfect candidate for different composites. Given that GO itself has a few limitations; poor colloidal stability and weak compatibility. Thereby the properties of GO can be enhanced by incorporating nanomaterials with varying characteristics [8]. Consequently, making graphene oxide-based composites a multidimensional material,

exhibiting synergistic physiochemical properties and revolutionizing the environmental techniques. Some of these reported nanomaterials are depicted in **Figure 1.2**.

Graphene oxide-based composites can thus be used as sensors, antimicrobials, photocatalysts, and sorbents [9]. As a result of their high surface area, and functionality, they have excellent adsorption and absorption capabilities. Hence various pollutants from both liquid and gases can effectively be removed by making them insoluble due to chemical or physical binding with GO-based composites [10], [11]. Furthermore, to facilitate the degradation of chemical pollutants, graphene oxide-based nanocomposites can be tuned to harness a broad sunlight spectrum. Their excellent ability to readily generate electron-hole pair initiates redox reaction hence breaking down the contaminants into less harmful byproducts [12], [13]. Additionally, their selectivity and specificity against various contaminants make them ideal for different sensors. Such as electrochemical, optical, or mechanical [14], [15]. Lastly, with several modes of action and the ability to adjust toxicity against pathogens GO-based nanocomposites are a promising alternative to conventionally used antimicrobial agents [16], [17]. Possible by simply adjusting the structure and dimensions of the composite.

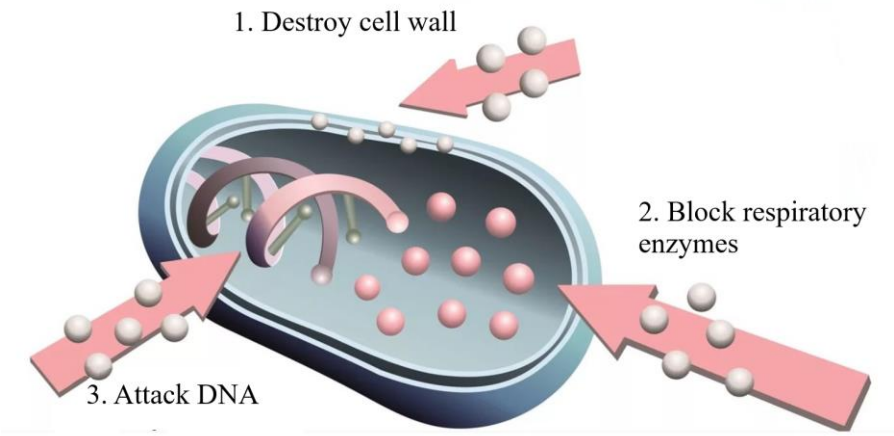

Figure 1.3: The mode of action of AgNPs on microbials.

Sliver nanoparticles (AgNPs) are currently the most investigated and commercialized biocides due to their exceptional antimicrobial susceptibility [18]. With

several mechanisms of action due to direct interaction with the microbe and release of silver ions (Ag^+). As such AgNPs facilitate the production of reactive oxygen species (ROS), block respiratory ions, interference with DNA replication, and physical disruption and damage of the cell wall or membrane [19] as briefly shown in **Figure 1.3**. Hence, even though they are still under investigation AgNPs have proved to be effective against "super-bacteria" created by excessive use of various antibiotics [20].

Furthermore, AgNPs have versatility in sensing, photo-catalytical, disinfecting, and sorbent capabilities. They are utilized in coatings, surface-enhanced Raman spectroscopy (SERS), breakdown of organic pollutants, and removal of heavy metal ions or other pollutants, along with various other applications [21], [22]. However, the effectiveness of AgNPs is limited because they tend to oxidize and aggregate thereby reducing their active surface area [20]. Graphene oxide-silver (GO-Ag) composites demonstrated a significant enhancement in the effective inhibition of microbial along with sensing and removal of pollutants. Therefore, the decoration of GO with AgNPs is a novel yet effective approach to tackle the ever-increasing environmental concerns. Especially since the specific properties required for various applications can be optimized by varying the shape, size, and charge on the surface of these composites or by choosing the appropriate synthesis approach. Among the current synthesis methods pulsed laser ablation in liquid (PLAL) is an attractive technique because of its robust experimental setup providing a simple, clean, fast reaction and surfactant-free product. Moreover, the characteristics of the AgNPs on the GO matrix can be effectively controlled by varying laser parameters such as time of ablation and pulse laser energy. While maintaining the integrity of the GO matrix.

Accordingly, this thesis focuses on the formation of a high-quality GO-Ag-based composite through the PLAL method. To understand their physiochemical properties by characterization and to study the impact of different laser parameters on the shape and size of the composite. Along with the optimization of these parameters. Furthermore, their evaluation as SERS and antibacterial agent, against both gram-negative and gram-positive bacteria thus confirming their multifunctional capabilities for environmental remediation.

CHAPTER 2: LITERATURE REVIEW

2.1 Introduction

Though the breakthrough of graphene was a mere accident, it has changed the course of scientific research and development. Known as the thinnest material it consists of a monolayer of sp^2 hybridized carbon atoms arranged in a hexagonal structure [6]. It exhibits high surface area and exceptional electrical, mechanical, and thermal properties. Moreover, the structure of graphene can be transformed into various dimensional materials [23], as shown in **Figure 2.1**.

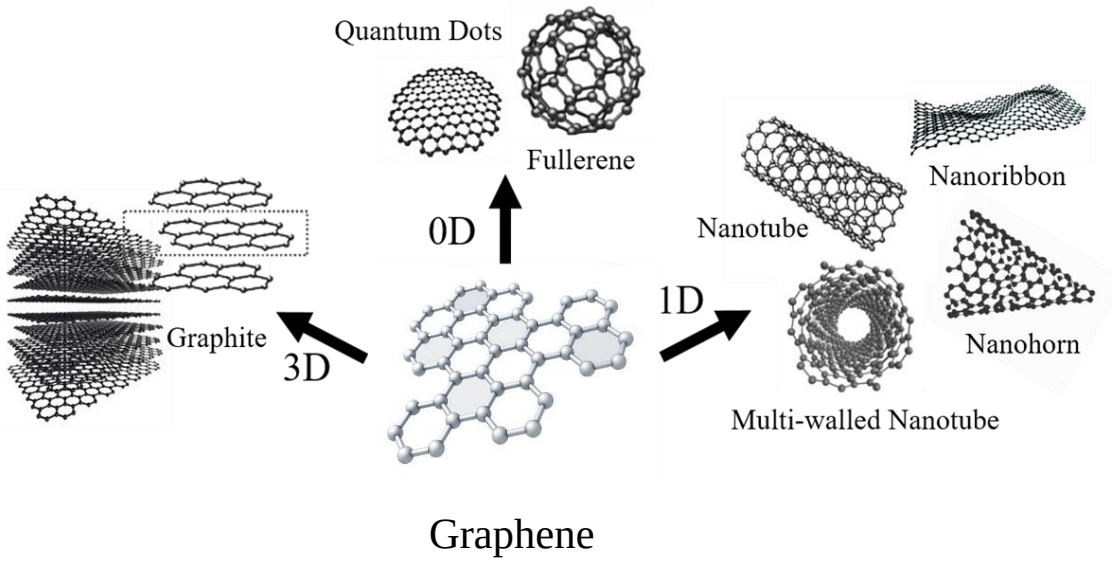

Figure 2.1: 0D, 1D and 3D carbon material formed from 2D graphene.

However, due to the hydrophobic nature of graphene, dispersing it in polar solvents is challenging. Whereas, graphene oxide a functionalized derivative of graphene has an enhanced interaction with polar solvents thus better dispersibility. Thereby GO preserves the unique properties of graphene along with improved characteristics due to oxygen-

functionalization. Thus, GO has better biocompatibility, dispersibility, stability, chemical reactivity, and optical and mechanical properties. As such it is a trending material in various fields of research such as sensors, catalysis, energy storage, biomedical, and environmental remediation.

2.2 Graphene Oxide

Graphene oxide is characterized by multiple or monolayer of graphene sheet with oxygen functionalization such as carboxyl, epoxide, and hydroxyl groups. These groups contribute to the negative charge, stability, interactions, and attachment of other substances with GO as explained in **Figure 2.2**. Thereby modifying the electrical and mechanical properties. Furthermore, GO is low-cost, scalable, and accessible thus being suited for novel composite materials [24].

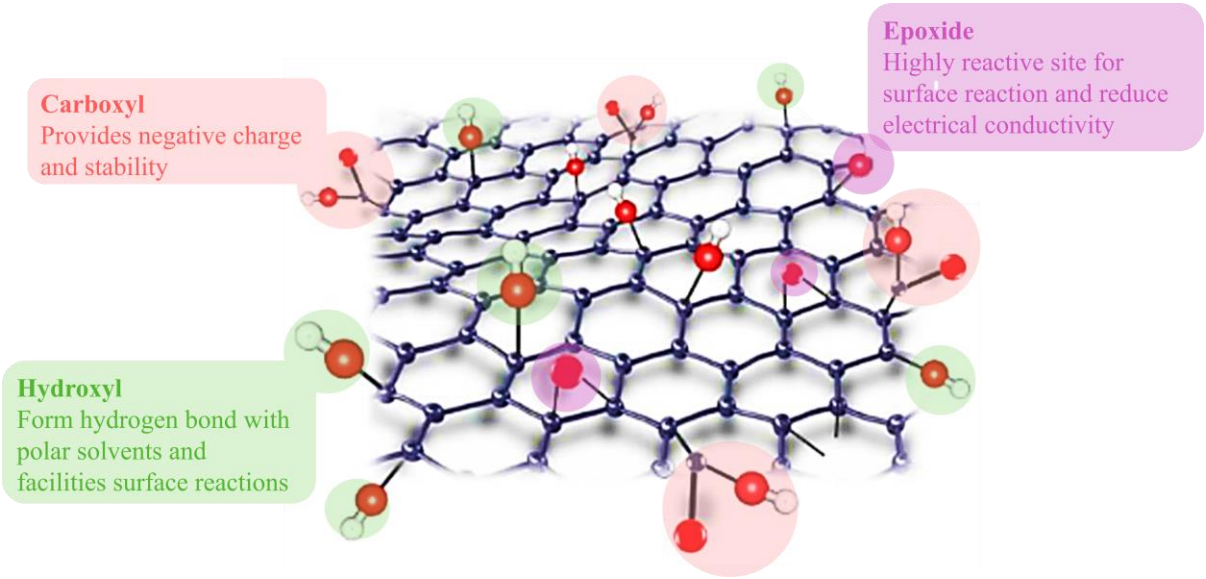

Figure 2.2: Schematic of GO sheet.

2.2.1 Synthesis of GO

Graphene oxide can be derived from graphite flakes or powder which can be obtained from natural and synthetic sources. Natural sources are preferred due to the presence of localized defects in the structure which act as seeding sites for various chemical

reactions. Generally, two approaches can be opted for the formation of GO, top-down and bottom-up. The bottom-up approach includes the production of GO through processes like Chemical Vapor deposition (CVD) where a controlled single layer of GO is deposited onto the selected substrate [25]. Whereas, the most preferred top-down approach aims to exfoliate or cleave graphite by chemical, physical, or mechanical processes. Brodie, Staudenmaier, or Hummers method and their modifications are used to carry out the oxidation of graphite for successful chemical exfoliation.

For Brodie's method potassium chlorate ($KClO_3$) with nitric acid (HNO_3) is used for the oxidation process [26]. This yields highly oxidized GO although the process is time-consuming as well as dangerous. Due to the release of toxic chlorine dioxide (ClO_2) gas which is highly explosive in nature. Staudenmaier modified the Brodie method by incorporating sulfuric acid (H_2SO_4) thereby oxidizing the graphite flakes in a shorter time [27]. However, it still had the same drawback of being dangerous.

Whereas, the Hummers' method utilizes Potassium permanganate ($KMnO_4$) and sulfuric acid (H_2SO_4) as oxidizing agents. Strong acids such as HNO_3 and H_2SO_4 lead to the formation of graphite salts which act as precursors for subsequent oxidation of GO [28]. Hummer's method is comparatively safe and efficient hence it is the most frequently used method to prepare GO. Although it does not produce any explosive gas, the hummer's method needs to be well controlled to avoid producing a highly exothermic reaction. Furthermore, it results in hazardous gases and magnesium compounds which need to be properly disposed of to avoid environmental contamination. Therefore, hummer's method has been modified to avoid the formation of these gases thus making is more eco-friendly. Chen et al designed a modified hummers' method by using H_2SO_4, $KMnO_4$, and $NaNO_3$ for oxidization [29]. Whereas Marcano et al formed the Improved Hummers' method by utilizing H_2SO_4, $KMnO_4$, and H_3PO_4 as oxidizing agents [30]. This green, cost-friendly, and low-waste process produces a high yield of hydrophilic GO due to gentle exfoliation, without damaging the hexagonal structure and without the release of any toxic gasses [5], [31]. Additionally, to control the purity, and quality of GO with enhanced colloidal stability synthesis parameters; temperature, reaction time, washing, and neutralization can be controlled and optimized [32], [33], [34].

2.2.2 Applications of GO

Depending on the functionalization of GO it can be incorporated into various broad applications. Such as energy storage, water purification, sensors, biomedical applications, catalysis, coatings, films, and electronics. Due to high surface area and electrical conductivity, GO has enhanced the storage capacity and stability therefore it is widely used as batteries and supercapacitors. Exponential research is being done to demonstrate GO-based nanocomposites' ability to perform as supercapacitors, lithium-ion batteries, and fuel cells [35]. Dong et al formed graphene-based platinum (Pt) and platinum-ruthenium (Pt–Ru) materials for fuel cell application by oxidation of methanol and ethanol [36]. Rakhi et al fabricated GO decorated with metal oxides with enhanced specific capacitance and stability of over 6000 cycles. Thereby being excellent for energy applications [37].

Additionally with exceptional adsorption properties GO is vastly used for the removal of various contaminants from water. These include heavy metals and pathogenic and organic pollutants. Therefore, it can be utilized in membrane technology and advance water treatment systems [38], [39]. Han et al demonstrated a vacuum-assisted filtration system based on an ultrathin GO membrane of a few nm porous polymer by using a trace amount of GO. The results showed 99% filtration of organic dyes and high water permeance [40].

2.3 Silver Nanoparticles

Notably among the diverse range of nanomaterials, noble metal nanoparticles have gained immense attention due to their distinctive physical, optical, chemical, and biological properties. Therefore, allowing researchers to incorporate them in various devices. In the case of silver (Ag), gold (Au), copper (Cu), etc, the intense colors are due to collective oscillations of free electrons in the conduction band. This phenomenon is known as Surface Plasmonic Resonance (SPR). Depending on the size and shape of the colloidal nanoparticles the color is varied [41]. Furthermore, since the SPR frequency is in the visible range they are utilized in serval optical applications such as biosensors [42]. Additionally, they are used for the treatment of cancerous tumors [43], drug delivery [44], catalysis [45],

and as various sensors such as SERS [46]. Due to their capability of creating ‘Hot Spots’ where enhancement of electromagnetic radiations takes place.

Among all the noble nanomaterials, silver nanoparticles have exceptional environmental remediation properties. Due to various physiochemical characteristics such as excellent thermal and electrical conductivity, SERS, catalysis, non-linear optical properties, and chemical stability [47]. Furthermore, it has superior antibacterial, and sensing capabilities [48]. Additionally, it is a cost-effective noble nanomaterial that can be synthesized through various optimized methods with varying shapes and sizes. Therefore, it is the optimal nanomaterial for the formation of GO-based nanocomposites for environmental protection.

2.3.1 Synthesis Methods

Silver nanoparticles can be synthesized by two different approaches just like GO. The first bottom-up method builds up individual atoms into nanoparticles. While the second, top-down, macroscopic materials are carved or broken down to produce nano-sized particles. Both approaches have various synthesis techniques as portrayed in **Figure 2.3**. Among these Pulsed Laser Ablation in Liquid (PLAL) is the most simple, effective, and clean method for generating AgNPs. Since no surfactant or other chemicals are required for the formation of well dispersed, few nanometre, bare AgNPs. Therefore, not compromising any of their unique properties due to the availability of all the active sites on the surface of these NPs. Furthermore, through PLAL the size, shape, and distribution of AgNPs can be optimized by varying parameters such as laser energy, pulse duration, and ablation time. Other common methods such as chemical reduction utilize silver salts and reducing agents which can cause serious health problems and can produce harmful by-products. While requiring capping agents and complicated purification processes [49]. Similarly, though biological methods are green in nature, they have longer synthesis processes, limited scalability, and control over the size and shape of the AgNPs. Along with the introduction of impurities and various ligands and surfactants due to the complex nature of biological components.

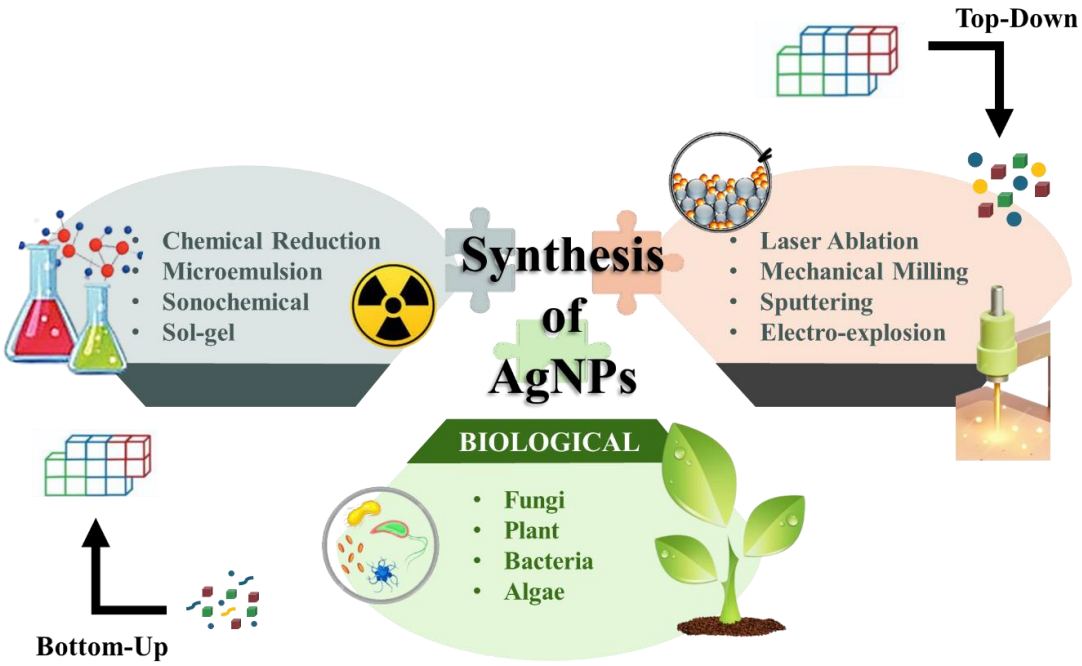

Figure 2.3 Nanomaterial synthesis approaches and techniques.

2.4 Pulsed Laser Ablation in Liquid

Pulsed laser ablation in liquid is a recently developed technique that can synthesize pure; ligand-free, and well-dispersed colloidal nanoparticles in a single-step process. Ever since Fojkit et al. first introduced it in 1993 [9] it has gained due interest and translated into several reviews [50], [51], [52], [53]. As presented in **Figure 2.4** a hybrid mechanism of top-down and bottom-up methods is employed for the formation of nanoparticles. Initially, in the top-down method, a high-energy pulsed laser beam breaks down the solid target immersed in a liquid medium. Consequently, causing material breakdown to produce a hot-dense plasma plume. Which expands as more material is broken down and as the laser interacts with the already produced plume to further increase the temperature and pressure. However, due to the liquid medium, the plume is quenched thereby causing the collision of ablated species with the liquid. This causes the formation of a thin vapor layer and the condensation of plasma species hence the start of the bottom-up process. So, forth the

nucleation of the initial seeds and subsequent growth into the resulting pure crystalline nanoparticles take place. While the vapor layer expands into a cavitation bubble and the plasma is extinguished. As the laser irradiation of nanoseconds (ns) is stopped till the next pulse the plasma can no longer maintain the high temperature and pressure and soon dies down. Similarly, during the expansion of the cavitation bubble, its temperature and pressure decrease than that of the surrounding liquids. Causing the collapse of the bubble and release of nanoparticles in the liquid.

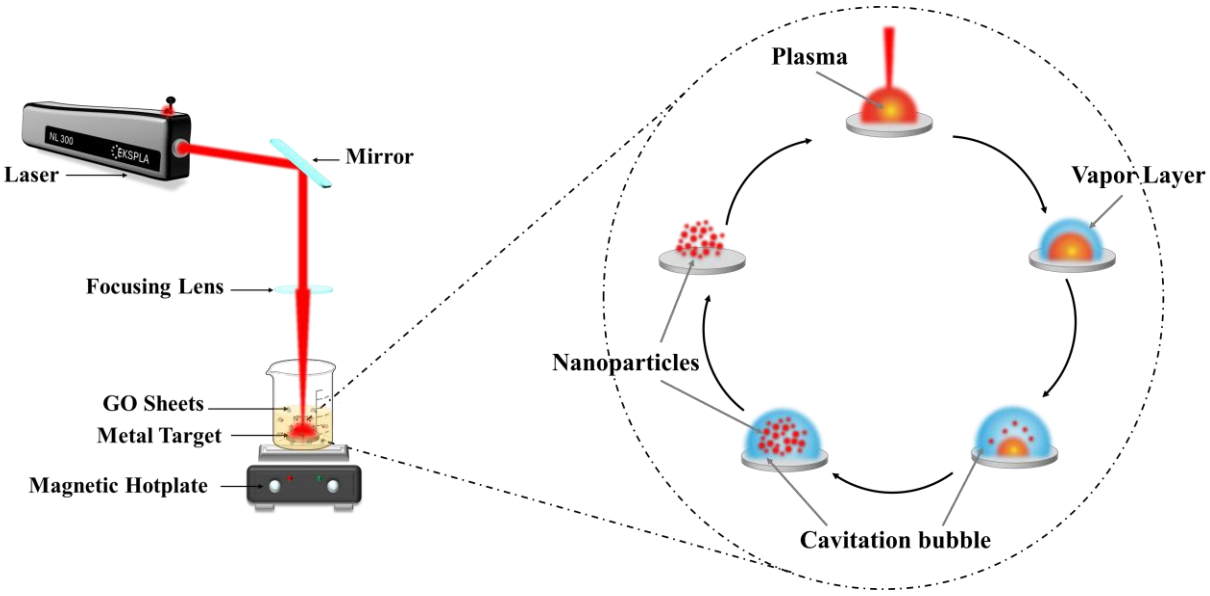

Figure 2.4: Schematics diagram of basic PLAL mechanisms.

PLAL is a versatile technique that can produce various nanoparticles such as metal, noble metal, oxide, composites, core shells, etc by simply varying the liquid medium and target material. Various researchers demonstrated the effect of different laser parameters on the synthesized nanoparticles. Tsuji et al investigated the effect on the fluence and ablation properties of Ag and Cu NPs by changing the focusing conditions and laser wavelength [54]. Accordingly, they found that high ablation efficiency is achieved at lower fluence and shorter wavelengths. Similarly, it can be achieved at longer wavelengths but at higher fluence. Moreover, smaller mean-size nanoparticles are synthesized by decreasing laser wavelength due to the fragmentation of the nanoparticles which interact

with the incoming laser pulse. Likewise, Zheng et al. demonstrated the effect of laser wavelength and laser power on the size and shape of the synthesized NPs [55].

The confining liquid plays a crucial role in the formation of nanoparticles. As it provides reactive species, confines and cools the plasma thus making nucleation possible. In addition, the surface charge of the forming nuclei is effected by the liquid species which in turn controls the size and agglomeration of the NPs. As reported by Mafune et al. by increasing the concentration of Sodium Dissolve Sulfate (SDS) in water, the average size and size distribution of NPs decreases [56]. Tarasenko et al. also demonstrated the surface modification of spherical AgNPs by utilizing acetone as the liquid medium [57]. Whereas AgNPs with improved stability were synthesized in natural polymer by Zamiri et al. [58].

Furthermore, laser fragmentation and laser melting in liquid can be employed for changing the shape and size of the synthesized NPs. As exhibited by Tsuji et al. submicron-sized AuNPs can be produced by laser melting in the presence of sodium chloride (NaCl) stabilizer [59]. Pyatenko et al. also reported the mechanism of the interaction of pulse laser with colloidal NPs [60]. Thus, presenting that the complicated laser-matter interaction process during the size reduction and spherical growth can be understood using the heating, melting, and evaporation model. Therefore, extensive research is being carried out to prove the versatility and simplicity of the single-step PLAL process to fabricate pure colloidal solutions. Without the use of any reagents and through a clean reaction; that produces no by-products.

2.5 Challenges and Limitations

A notable challenge with AgNPs is their prolong stability as they readily oxidize and aggregate over time. Thereby decreasing the active surface area and application-based efficiency. Therefore, it is necessary to incorporate them with other nanomaterials that can preserve and possibly enhance their inherent properties. Furthermore, the potential risks of AgNPs by leaching into the environment are still not fully understood however are still of significant concern and thus need to be addressed [61]. Subsequently, for appropriate

environmental remediation application of AgNPs with its unique characteristics and challenges it is infused with GO to form a composite with enhanced properties.

2.6 Graphene Oxide-Silver (GO-Ag) Nanocomposites

To overcome the challenges of GO and AgNPs while having synergistic properties with high surface area various researcher are being carried out on the formation of GO-Ag nanocomposites. GO provides anchoring of AgNPs thereby preventing the possibility of aggregation and resulting in higher colloidal stability. Hence having improved properties for various applications such as antibacterial, sensing, and catalysis [62].

2.6.1 Synthesis Methods for GO-Ag Composites

Various methods for the synthesis of GO-Ag have been explored [63] however PLAL is a much preferred technique to the robust experimental setup and easy process. Furthermore, a well-dispersed colloidal composite is achieved with AgNPs homogenously anchored on high surface area GO sheets. Therefore, enhanced stability and functionality of the composites are exhibited without the introduction of any chemical additives and by-products. Whereas the other in-situ methods such as chemical reduction [64] and microwave irradiation require various additives and complicated experimental setups. Additionally, optimizing the size, density, and shape of the composites is challenging with mostly reduction of GO [65], [66]. Whereas PLAL is relatively the most eco-friendly and green technique. Moreover, the shape, size, and distribution of the composite can be controlled by optimizing the laser parameters. Thereby having optimal performance in environmental applications.

As demonstrated by He et al., PLAL can be utilized for decorating GO sheets with AgNPs while controlling the size and density of NPs by varying laser parameters [66]. Hence improving the Ag nanoparticle/GO catalysis and SERS capabilities. Similarly, Menazea et al, reported the formation of copper and silver nanocomposites with GO (AgNPs@GO and CuONPs@GO) while focusing on demonstrating their photoactivated antibacterial activity [20]. Likewise, Nancy et al. fabricated Ag-GO nanohybrids with excellent antibacterial activity and nonlinear optical properties [19]. With the formation of

intermediate energy states. Furthermore, showing the versatility and reduction capabilities of PLAL Al-Assaly et al. produced rGO decorated with AgNPs using the PLAL method [67]. They optimized the laser pulse energy and the ablation time for forming uniformly dispersed AgNPs on rGO sheets. Subsequently, Malik et al. synthesized Ag-GNPs with varying weight ratios through an ex-situ approach to demonstrate photocatalytic potential and antibacterial susceptibility against various bacteria [68].

2.6.2 Applications of GO-Ag Composites

With enhanced electrical conductivity, increased active surface area, and strong application-based activities GO-Ag composites have proved to be multifunctional materials as displayed in **Figure 2.5**. It can exhibit effective and excellent performance against environmental pollutants and pathogens. As such GO-Ag composites have shown an improved antibacterial activity against gram-negative and gram-positive 'super bacteria' than that of their individual components. Especially when the increase in antibiotic resistance of bacteria is an ever-growing health concern. Uniform distribution of AgNPs on GO sheets prolongs the activity of GO-Ag composite due to enhanced stability, and availability of AgNPs. Furthermore, it prevents the restacking of GO sheets and agglomeration of AgNPs. Additionally, the anchored AgNPs readily realize Ag+ ions which are known to contribute to the activity of AgNPs by disturbing the cell wall, causing oxidative stress due to ROS, and interfering with the replication of DNA For instance, Truong et al reported superior antibacterial activity of GO-Ag NPs against E. coli and S. aureus bacteria due to the production of strong ROS species, and improved bacterial adhesion that leads to cell death [69]. Lange et al. demonstrated the cell death was caused by GO-Ag nanocomposite by disruption of the cell membrane, oxidative stress, and peroxidation of lipids [70]. Furthermore, they reported GO-Ag nanocomposite use as a textile coating.

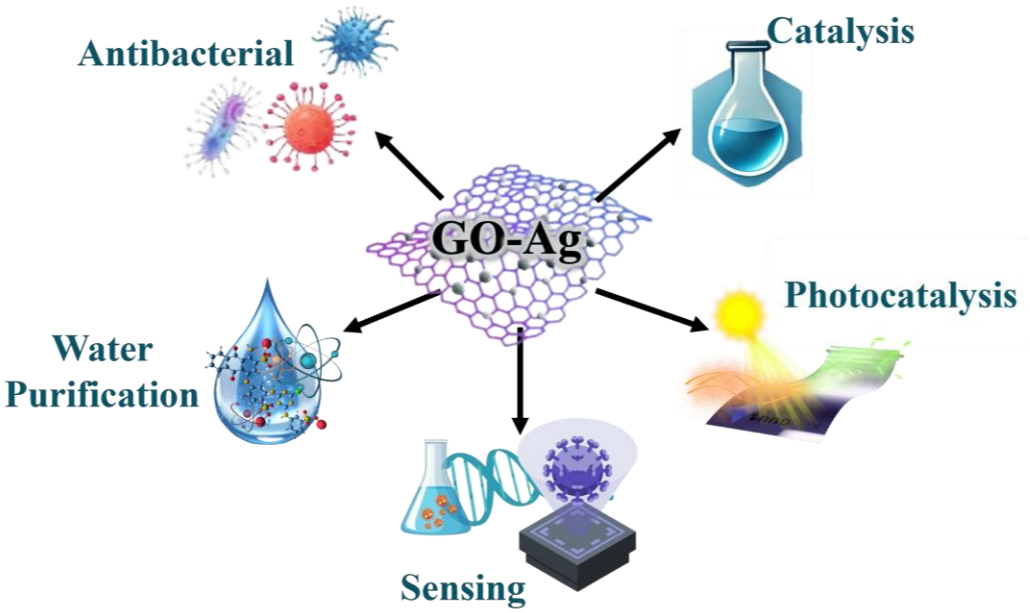

Figure 2.5: Applications of multifunction GO-Ag composites.

GO-Ag composites have proved to be applicable in water purification systems for environmental cleanup. Due to the high surface area, GO-Ag composites are excellent absorbents for organic pollutants and heavy metal ions. As demonstrated by Naeem et al. GO-Ag can be used to effectively adsorb industrial dyes such as methyl orange (MO), methylene blue (MB), and ethyl violet (EV) [71]. Along with the reduction of aromatic pollutant 2-nitroaniline (2-NA) and antibacterial activity against E. coli and S. Aureus. Likewise, Dandu et al. formed a GO-Ag composite for the removal of Pb(II) ions [72]. The reported removal of ions depended on the pH, concentration of ion, dose of adsorbent, and time of contact. However successful removal of Pb(II) ion was achieved from both water and wastewater. The adsorption capabilities of nanocomposite have been linked to the functional group of GO-Ag since they interact with the heavy metal ions. Through the process of ion exchange and electrostatic interaction to form surface complexes. Therefore, increased specific surface area by deposition of AgNPs enhances the overall adsorption of the ions [72], [73].

Moreover, AgNPs decoration of the GO sheet changes the bandgap of the composite thereby enhancing the electron-hole pair generation upon light irradiation. This results in an improved photo catalytical activity for the breakdown of complex organic dyes, without the production of other hazardous by-products [74]. In research conducted by Zhong et al., a ternary silver/bismuth oxyiodide/graphene oxide (Ag/BiOI/GO) composite was prepared for the removal of rhodamine B (RhB) dye under the exposure of visible light[75]. They demonstrated the stability and reusability of the synthesized composite due to the inhibition of the recombination of electron-hole pairs by the doping of AgNPs and GO.

Exponential research on incorporating GO-Ag composite in sensing applications is being carried out. Particularly for sensitive and selective chemical and biosensors. Upon addition of AgNPs on the GO sheet, their SPR properties can easily be exploited to sense various molecules with prolonged use due to added stability and enhanced characteristics. Zhang et al successfully constructed an electrochemical sensor using AgNPs/GO composite for the detection of dopamine (DA) and hydrogen peroxide (H_2O_2) [76]. Thereby demonstrating the increase in specific surface area increased the sensitivity, decreased the detection limit, and showed exceptional reproducibility and stability. Nguyen et al. also developed green silver-doped graphene oxide (AgNPs@GO) nanocomposite to demonstrate high H_2O_2 and Hg^{2+} detection through optical sensing [77]. Along with low detection limits, thus presenting it as an ideal colorimetric sensor. He et al. reported Ag/GO composites exhibit excellent (SERS) capabilities due to the anchoring of AgNPs on GO sheets [66]. Thereby providing stability, enhancing plasmonic activity, and creating "hot spots" with a strong electromagnetic field which in turn increases the Raman signal significantly while decreasing the limit of detection of various analytes such as Rhodamine 6G (R6G) and 3,3',4,4'-tetrachlorobiphenyl (PCB-77) [66].

CHAPTER 3: MATERIALS AND METHOD

The experimental work has three distinctive phases.

Experimentation	**Synthesis or formation of** GO through Improved Hummer's Method (Tour's method) GO-Ag nanocomposites through PLAL
	Charaterization of Material FTIR UV Vis spectroscopy XRD SEM RAMAN spectroscopy Zeta Potential
	Application-based testing GO pH dependant antibacterial Composites' shape dependant antibacterial Surface Ehnaced Raman spectroscopy

3.1 Synthesis and formation

3.1.1 Graphene Oxide

The chemical exfoliation method was opted to form graphene oxide due to its cost-effectiveness, ease, and sustainability. To maximize product yield and quality, graphene oxide was synthesized from graphite flakes through the Improved Hummer's Method [30], as briefly exhibited in **Figure 3.1**.

In this procedure, 1.0 g graphite flakes were mixed with a 9:1 mixture of concentrated H_2SO_4/H_3PO_4 (120:13.3 mL) solution and stirred for 30 min. Following that $KMnO_4$ (6.0 g) was gradually added to the mixture making it turn green. The temperature

was kept below 35-40° C and the reaction was further stirred for 4-5 hours. Then the reaction was heated to and maintained at 50° C for 12 hours under constant stirring. Afterwards, the reaction was allowed to cool down to room temperature and poured onto ice and 30% H_2O_2 (1 mL) to quench the reaction. Completion of the reaction yielded a bright yellow solution, confirming the successful formation of graphite oxide. Before the washup to remove the unreacted graphite flakes, the solution was sifted through a laboratory test sieve. The filtrate was then centrifuged at 4000 rpm to separate the solid material from the acidic supernatant. Subsequently, it was washed successively with 67 mL 30% HCL and ethanol to remove the unwanted metal ions. Further washing was carried out several times with DI water to increase the pH of the product to attain a different pH. The final product was dried out overnight at a low temperature (40-60° C) to obtain graphene oxide powder, without affecting its chemical structure.

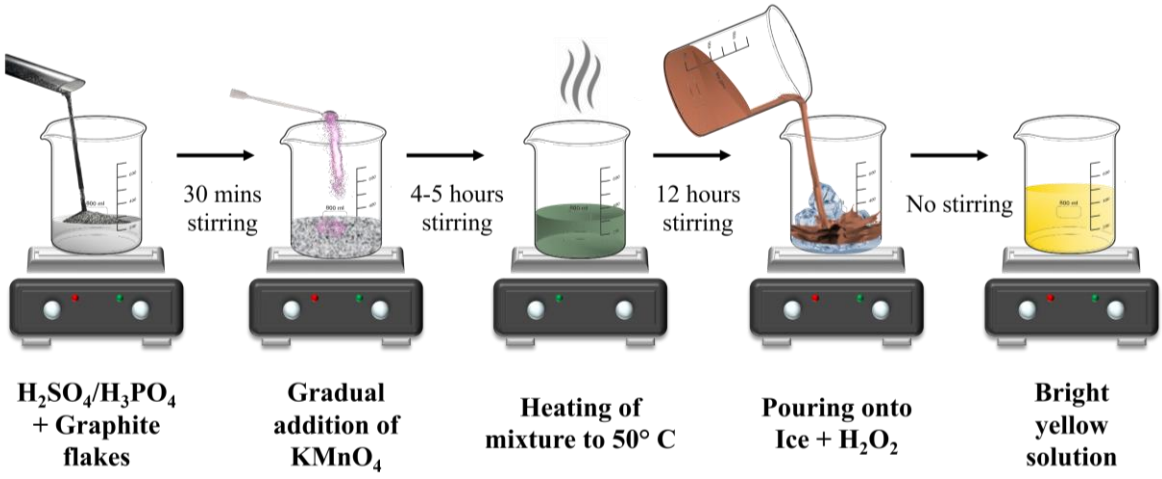

Figure 3.1: Schematic diagram of Improved Hummer's Method.

3.1.2 Graphene Oxide-Silver Nanocomposites

To synthesize optimum GO-Ag nanocomposite, the fabrication process was further divided into two individual stages. **Figure 3.3** depicts the basic Pulsed Laser Ablation in

Liquid (PLAL) setup consisting of an Nd-YAG laser, beam-delivering optics, and a vessel to hold the solvent and the target.

- First Stage

Initially, graphene oxide of a pH of 5.5 was dispersed in DI water at a concentration of 0.2 mg/mL. Two different DI waters were utilized for the sonication process. To avoid the thermal reduction of GO, the suspension was sonicated in an ice/water bath while maintaining a temperature below 20° C. The beaker with GO suspension was covered to avoid any unwanted contamination and immersed in the water of an ultrasonication bath Elma Schmidbauer E 30 H, Germany. As briefly shown in **Figure 3.2**. Depending on the suspension volume the sonication was carried out for a minimum of four hours. Sonication in a vial was avoided as the heat and pressure generated during prolonged sonication would erupt the vial.

Figure 3.2: Sonication of GO solution in ice/water bath.

➢ Second stage

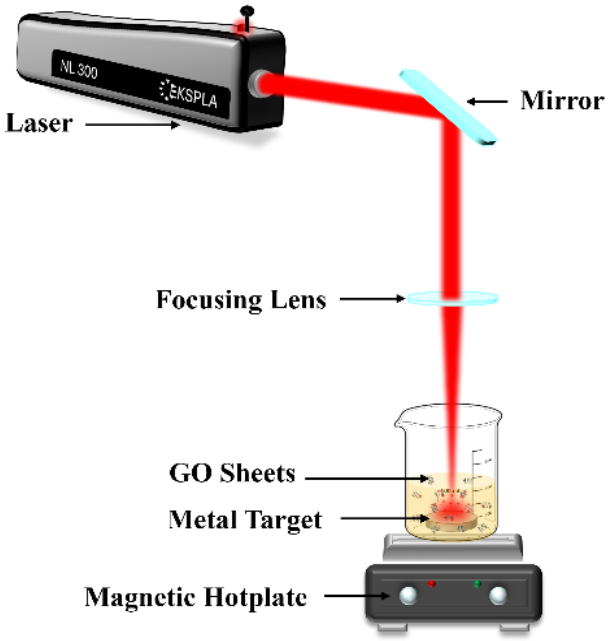

Figure 3.3: Schematic diagrams of the PLAL experimental setup.

Following the sonication process the silver target was polished to remove all accumulated impurities. It was then thoroughly washed with ethanol and distilled water and immersed in a beaker with 4 mL of sonicated GO solution. Subsequently, it was placed on a magnetic hotplate for continuous stirring of the solution. The position of the beaker was physically changed after a few seconds to provide rotation of the target sample, which is essential for avoiding the formation of a deep ablation crater. Finally, the target ablation process, as illustrated in **Figure 3.3**, was carried out according to the laser parameters presented in Table 3.1 for the formation of GO-Ag composites. For shape optimization of GO-AgMC laser energy was varied from 106 mJ to 172 mJ while keeping the ablation time constant at 10 mins. Whereas the ablation time was varied from 5 min to 15 mins while keeping the laser energy constant at 140 mJ.

Laser Specification	
Laser type	Nd-YAG ns-Laser
Wavelength	1064 nm
Pulse duration	6 ns
Repetition Rate	10 Hz
Pulse Energies	106 mJ-172 mJ
Lens Focal length	50 cm
Ablation Time	5-15 mins

Table 3-1: Laser parameters for the synthesis of GO-Ag composites.

3.2 Characterization of Materials

3.2.1 Fourier Transform Infrared Spectroscopy (FTIR)

FTIR analysis of powder GO was performed to investigate functionalization of GO through Perkin Elmer, spectrum 100 FTIR spectrophotometer. FTIR of GO-Ag composites was avoided since these samples are prepared in dispersion form. Thus, the water content present in the samples interfered with the sample characteristics peaks. Causing them to broaden into a round shape. Therefore, the true spectrum could not be obtained. For the FTIR analysis, the GO powder was mixed with Potassium Bromide (KBr) and turned into a pellet using a hydraulic press. The spectrum was obtained in transmission mode with a scan ranging from 400 cm^{-1} to 4000 cm^{-1}.

3.2.2 Ultraviolet-Visible spectroscopy (UV-Vis)

GO and GO-Ag nanocomposites UV-Vis absorbance spectrums were obtained by UV-2800 BMS Scientific Technical Corporation (PVT) LTD. For performing the UV-Vis analysis, all the samples were diluted using the initial solvent (DI water) to avoid the irregular spikes present in UV-Vis spectra at high concentrations. Therefore 0.2 mL of the prepared sample and 1.8 mL of DI water was introduced into the quartz cuvette with an optimal optical path of 1 cm. The range of the analysis was limited between 200-800 nm. The obtained data was used to find the bandgap of the samples through Tauc's equation.

3.2.3 X-ray Diffraction (XRD)

XRD model theta-theta STOE, Germany was utilized for analysing the crystallinity of all the materials. Since the nanocomposites are formed in dispersion forms GO was dispersed in DI water. 20 times 10 μL of all the prepared samples were drop cast onto a clean glass slide to form a thick coating. The XRD analysis was performed at 2θ range from 0°-90° degrees, at a slow scan rate (45 mins). The obtained data was plotted and compared using X'Pert high-score software.

3.2.4 Scanning Electron Microscopy (SEM) and Energy Dispersive Spectroscopy (EDS)

for visual confirmation of GO, and GO-Ag nanocomposites Scanning electron microscope JEOL JSM-6042 A, Japan was utilized. With a working distance of 10 mm, 5kV acceleration voltage, and various magnifications. Furthermore, EDS analysis for elemental mapping was performed to confirm the elemental composition of some of the samples. For the sample preparation, 10 μL of the colloidal solution was deposited onto a cleaned glass slide and dried on a hotplate for a few minutes.

3.2.5 Raman Spectroscopy

For assessing the structure properties, degree of defects, and functionalization I-Raman, USA was used. Similar to the XRD analysis multiple depositions of the prepared samples were done on a clean slide to obtain a thick coating. Each sample analysis was conducted using a laser wavelength of 532 nm and power of 30 mW for 5 seconds.

3.2.6 Zeta potential

For the analysis of the surface charge and the stability of all the synthesized colloidal material dispersed in DI water, zeta analysis was performed using Zeta Potential Analyzer WALLIS ZPA220901, France. For zeta vs pH reading the 0.7 mL of the dispersed samples were added in a 2 mL quartz cuvette. Since the electrode must be dipped into the sample for accurate reading. The parameters were set; solvent as DI water, pH of 5.5, and the analysis was repeated three times.

3.3 Application-based testing

3.3.1 Antibacterial Assay

All antibacterial tests were carried out using *Escherichia coli PSU-5266 (E. coli)* and *Staphylococcus aureus BL 21* (S. aureus) due to the availability and extensive literature of the strains. Both strains were cultured in Lauria broth (LB). Briefly, primary inoculum was prepared by inoculating 1 colony from the streaked plate in 10 mL LB broth and incubated overnight in a shaking incubator for the equal division of cells. The secondary inoculum was prepared to bring the bacterial cells into the log phase (growth phase). 10 µL of the primary inoculum was added to 10 mL of LB medium and incubated in a shaking incubator for 2-3 hours. Thereby achieving an optical density of 0.6 at 600 nm by a spectrophotometer. Indicating the bacterial culture is in the growth phase thus further experiments could be performed [17].

3.3.1.1 GO pH-dependant antibacterial

GO antibacterial susceptibility is influenced by purity therefore the pH was adjusted during the washup and through post acid/base addition.

Materials required

- GO 0.5 mg/mL
- Ascorbic Acid ($C_6H_8O_6$)
- Sodium Bicarbonate ($NaHCO_3$)
- LB broth
- Eoisin Methyl Blue Agar (bacterial growth mediums).
- Pipettes
- Bacterial strains
- Petri dishes
- Eppendorf tubes
- Glass spreader

A. Plate Count Method

Multiple tests were performed to confirm the antibacterial activity of GO. Initially plate count method was utilized to confirm if neutral pH (5.5) GO has any antibacterial activity or not, as briefly represented in **Figure 3.4**. For which 1000 μL broth and 100 μL E. coli bacteria were added to nine Eppendorf tubes, each. Then different amounts of powder; 0.2 mg, 0.5 mg, and 2.0 mg, and dispersions, 0.2 mg/mL, 0.5 mg/mL, and 2.0 mg/mL, of GO were added to each Eppendorf tube. The tubes were then kept in a shaking incubator at 37° C for 24 hours. To complete the test from each Eppendorf tube 100 μL of inoculum was added to the petri and spread using a glass cell spreader after sterilizing it using a spirit lamp. The plates were further incubated at 37° C for 24 hours to check the bacterial growth on the plates.

Following that the same test was repeated with GO pH of 3, 4, and 5.5. The pH was varied during the washup of GO after exfoliation of graphite flakes through an improved Hummer's method and wasn't altered post-washup through acid.

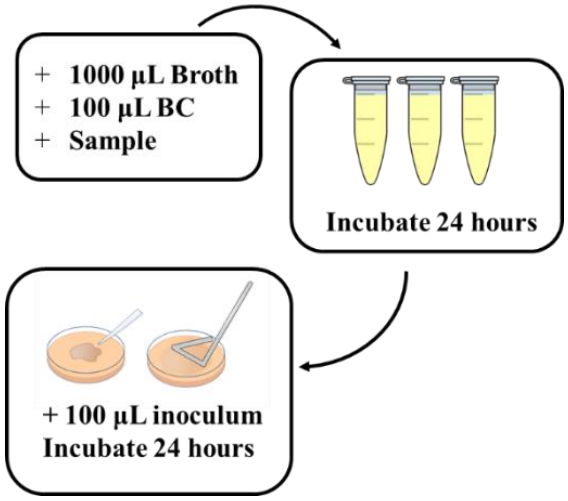

Figure 3.4: Plate count method for antibacterial assay.

B. 96 well plate test

Further confirmation of the pH-dependent antibacterial activity of GO was achieved through the 96-well plate method. Initially during the washup GO of pH 3 and pH 5.5 was acquired. For post pH change, 0.2 mg/mL solution was well sonicated and divided into seven different vials. Dropwise ascorbic acid was added to neutral pH (5.5) GO to attain a pH of 3 and 4. While $NaHCO_3$ was dropwise added to achieve a pH of 7 and pH of 8.

For the 96-well plate test, 100 µL of LB broth was added to each well (as many rows and columns as required). Afterward, the 100 µL of the prepared sample was added to the first well and was properly mixed. 100 µL of the mixture was discarded so the final volume would be 100 µL in the well. For the second well of the row, 100 µL of the sample was added, mixed and the 100 µL was pipetted out. This 100 µL was then added to the next well in the row. This was repeated till the 6^{th} well to achieve concentration dilutions as displayed in **Figure 3.5**. Different samples were added to different rows. Following this 10 µL of bacterial culture was added to the 2^{nd} to 7^{th} well. The 1^{st} well, without any bacterial

culture, showed material interaction with LB broth while the last, the 7th well depicted overall bacterial growth. Thus, both acted as a control.

The first test was carried out using GO of pH of 3, 5.5 attained through washup, ascorbic acid, and GO of pH 3 through acid addition against the E. coli strain. The following test was carried out using ascorbic acid, sodium bicarbonate, acid, and base added pH of 3, 4, 7, and 8. Also, the pH of 5.5 (neutral) was attained by complete washup of the synthesized GO against E. coli and S. aureus bacteria.

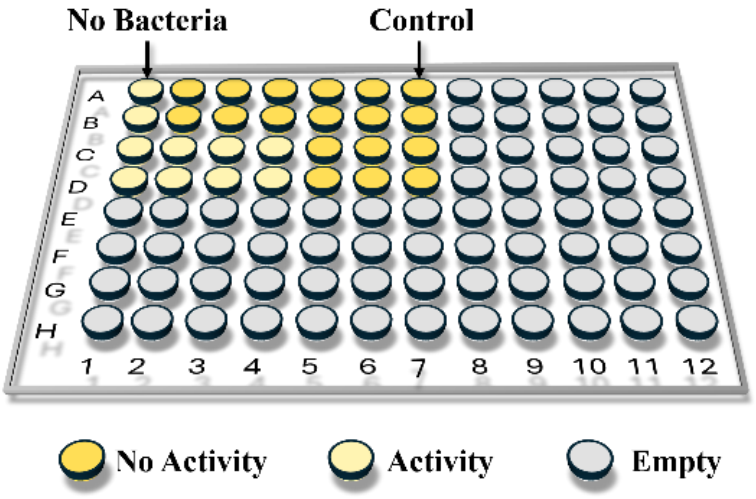

Figure 3.5: 96-well plate method for antibacterial assay.

3.3.1.2 Composites' shape-dependent antibacterial

Materials required

- GO 0.2 mg/mL
- TSC AgNPs
- GO-AgMC
- GO-AgNS
- LB broth
- Pipettes
- Bacterial strains

96 well plate test

Antibacterial activity of two different shapes and sizes of GO-Ag composites was evaluated against E. coli and S. aureus bacteria. While comparing it to the individual components; GO and AgNPs were synthesized through the improved method and PLAL, respectively. Furthermore, the antibacterial test of different GO-AgMC sizes synthesized at constant energy; 140 mJ while varying time from 5 min to 15 min was carried out against E. coli. All the tests were performed following the previously discussed 96-well plate test procedure.

3.3.2 Surface Enhanced Raman Spectroscopy (SERS)

Material required

- Methylene blue
- DI water
- GO of 0.2 mg/mL
- TSC AgNPs
- GO-AgMC
- GO-AgNS
- Vials
- Glass Slides

A compact Raman spectrometer with a 532 nm laser wavelength was utilized for the SERS study. The sample was exposed for 5 secs with a power of 2.5 mW, following different reported literature. In short ethylene blue solution with a concentration of 1×10^{-6} M was prepared by dissolving 319.85 µg methylene blue powder in 1 litre DI water. **Figure**

3.6 demonstrates that to prepare the slides, 50 µL of the prepared GO and GO-Ag composites was dried on individual slides of 1 cm^2. Afterward, 50 µL of MB was dried on top of the samples. For reference only 50 µL of MB was dried on the slides to collect the Raman spectrum.

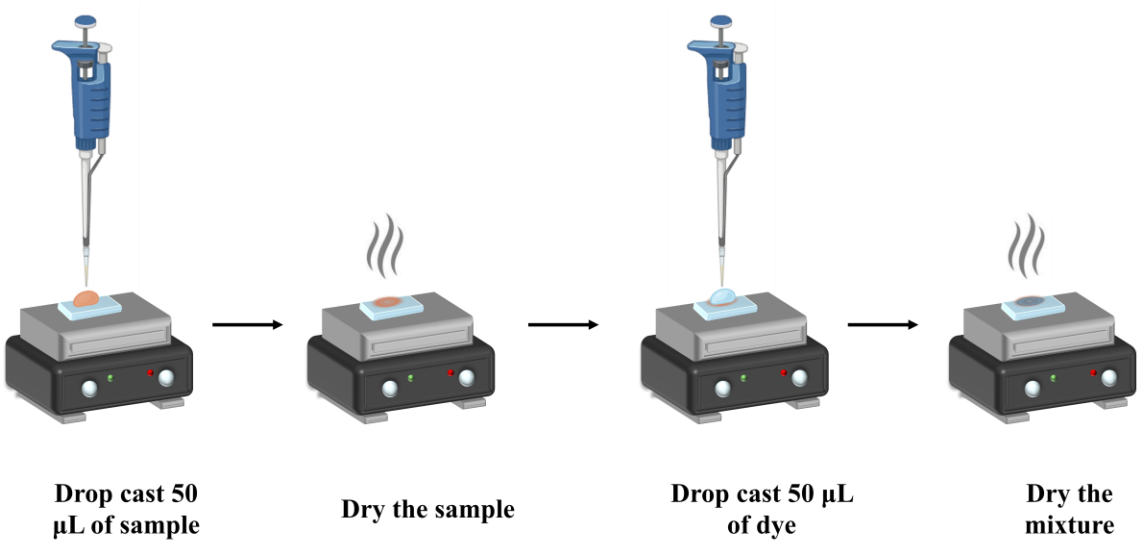

Figure 3.6: Schematic of SERS sample preparation.

CHAPTER 4: RESULTS AND DISCUSSION

4.1 Characterization of Materials

4.1.1 FTIR of GO

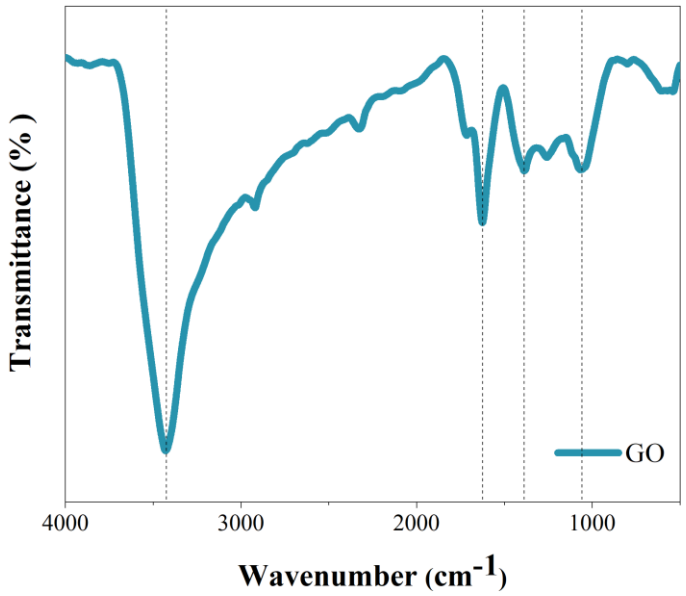

Figure 4.1: FTIR spectra of GO.

Figure 4.1 presents the distinctive absorption bands of all the oxygen-containing functional groups anchored on GO sheets. A sharp and broad peak around 3400 cm^{-1} is characteristically associated with the stretching vibrations of the O−H bond. During the chemical exfoliation process, these groups are attached to the basal plane and the edges of GO sheets. Therefore, a sharp hydroxyl peak represents extensive oxidation of GO by the improved hummer's method. Furthermore, the prominent 1600 cm^{-1} represents the C=C stretching vibrational band. This band is attributed to the sp^2-hybridization of carbon atoms in GO sheets thus proving the backbone of the graphene structure remains intact during the chemical exfoliation process and contributes to the overall structural integrity of the GO

sheets. Whereas the peaks at ~1300 cm^{-1} and ~1200 cm^{-1} are assigned to the stretching of the C−O bond due to the attached carboxyl and epoxy groups, respectively. These groups contribute to the hydrophobic nature and colloidal stability of GO in liquid mediums. Finally, the C−O−C stretching is correlated with the peak at near 1050 cm^{-1} which gives additional confirmation of the attachment of epoxy groups on the GO sheets [20], [67], [78]. The reactivity, interaction with other molecules, and functionalization capabilities of GO sheets are dependent on these oxygen-containing functional groups. Therefore, the spectra confirm the efficient oxidation of graphite flakes to produce highly oxygenated GO sheets which are an ideal substrate for the deposition of other nanomaterials.

4.1.2 UV-Vis of GO, GO-AgMC, and GO-AgNS

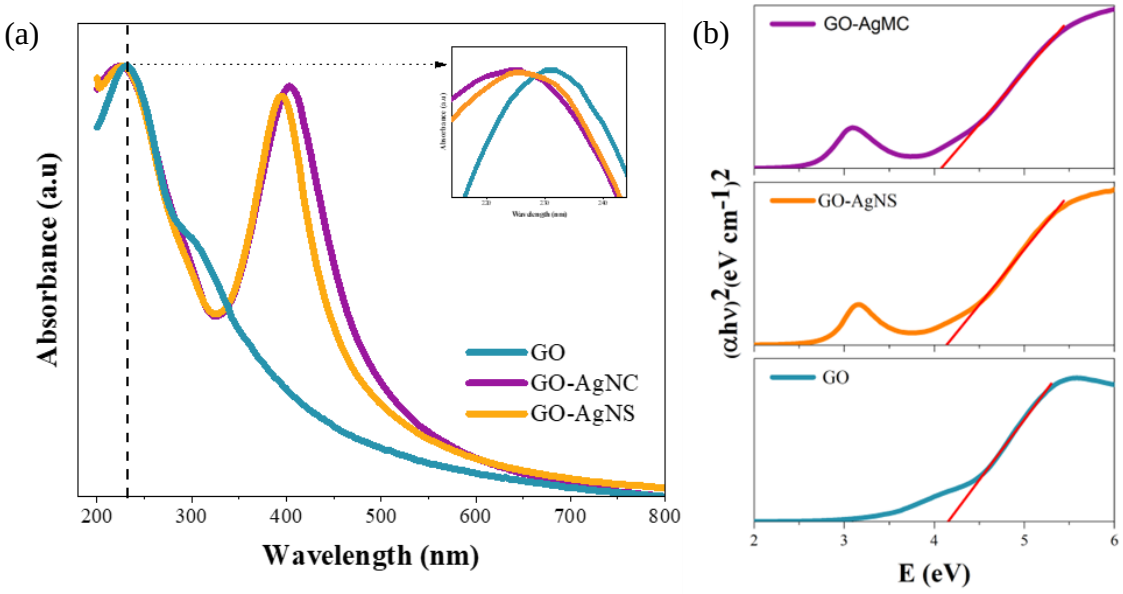

Figure 4.2: (a) UV-Vis spectrum (b) Bandgap of GO, GO-AgMC and GO-AgNS.

Figure 4.2 (a) graphically demonstrates the absorption spectrum of GO and GO-Ag composites synthesis by an improved method and PLAL, respectively. Pure GO exhibits an intense absorption peak at 232 nm, corresponding to the π→π* transition of C−C bonds, and a small shoulder peak at 302 attributed to n→π* transitions of C=O bonds. Indicating a high sp^2 hybridization of GO along with the presence of oxygen-containing

functional groups. Whereas, for the GO-Ag composites, a new adsorption peak is observed at 404 nm for cubic and 394 nm for the spherical, characteristic of the localized surface plasmon resonance (LSPR) of AgNPs. Thereby confirming the generation of AgNPs in GO solution and the formation of GO-Ag composites. Furthermore, as plotted in the inset of **Figure 4.2 (A)** a slight peak shift was observed in the GO absorption peak towards lower wavelengths. Indicating a change in the overall electronic conjugation of GO due to the interaction between GO and AgNPs. Subsequently, confirming that the irradiation with a pulsed laser did not reduce the GO sheets.

For the calculation of GO and GO-Ag composites bandgap Tauc's equation was used to plot the $(\alpha h\nu)^2$ vs $(h\nu)$ graph as illustrated in **Figure 4.2 (b)**. Mathematically Tauc's equation is expressed as:

$$(\alpha h\nu)^2 = A(h\nu - E_g)$$

Where α, $h\nu$, and E_g represent the absorption coefficient, energy of photon, and optical bandgap of the material. Whereas A is a constant of proportionality that varies according to the properties of the material. The interception of its linear part showed that upon the formation of GO-Ag composites, the band gap of pure GO decreases from 4.15 mV to 4.06 mV and 4.13 in the case of cubic micro-composite and spherical nanocomposites, respectively. Thereby improving the electron transfer between the valance and conduction band. This in turn could lead to an improved antibacterial activity of the composites.

4.1.3 XRD of GO, GO-AgMC, and GO-AgNS

The crystallinity of the prepared sample was determined through XRD. A single, sharp broad peak at 2θ of 11.5° for the (001) plane is observed for the GO powder sample as shown in **Figure 4.3**. To estimate the interplanar distance between GO sheet d-spacing is calculated using the Bragg's equation:

$$\lambda = 2d \times \sin(\theta)$$

Where λ, d, and θ represent the X-ray wavelength, the distance between planes present in the atomic lattice, and the angle between the incident and scattering ray. The GO peak corresponds to a d-spacing of 7.7 Å. Thereby suggesting the incorporation of various functional groups; epoxy, carboxyl, and hydroxyl within the planes of GO.

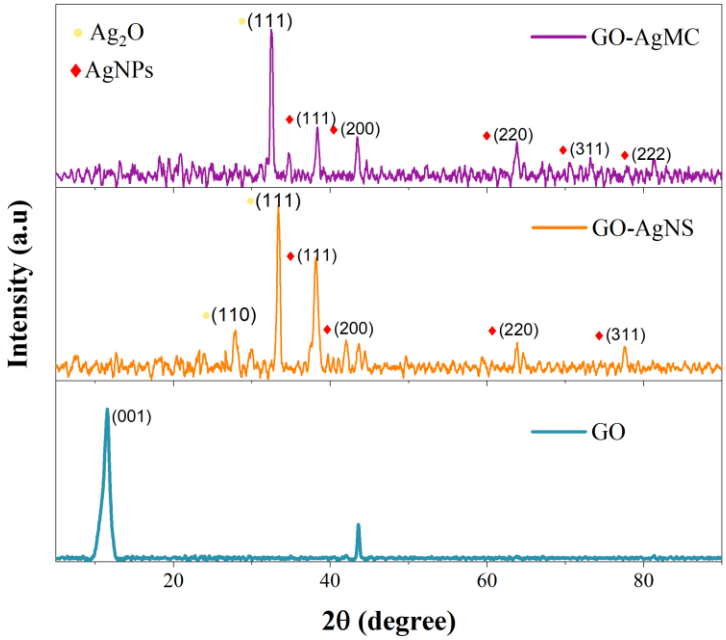

Figure 4.3: XRD spectrum of GO, GO-AgMC and GO-AgNS.

In the GO-Ag composites sample the GO peak became undetectable while the characteristic AgNPs and Ag_2O peaks were detected. This suggests the delamination of GO layers due to the prolonged sonication and deposition of AgNPs. GO-AgMC, exhibited peaks at 38.4, 43.4, 63.8, and 73.2, whereas GO-AgNS 38.1, 42.0, 63.8 and 77.5 of crystals (111), (200), (220), (311) and (222), respectively (JCPDS no. 04-0783). Furthermore, a sharp peak at 32.5 for GO-AgMC and at 27.9 and 33.3 for GO-AgNS indicated the presence of an Ag_2O crystalline (111) plane (JCPDS no. 76-1393). Suggesting a mixture of AgNPs and Ag_2O face-center cubic (fcc) structures are present in the GO-AgMC. Furthermore, the average crystal size of GO, GO-AgMC, and GO-AgNS was calculated using the Scherrer equation:

$$\beta = 0.93\lambda/(Lcos\theta)$$

Where the wavelength, full wave half maximum (FWHM) of the most intense peak, and the diffraction angle are represented by λ, L, θ [79]. Thus, the average crystal size is 8.9, 2.9, and 1.4 nm for GO, GO-AgMC, and GO-AgNS, respectively.

Additionally, since AgNPs are prone to oxidation it can be hypothesized that surface oxidation of AgNPs in a liquid medium caused the formation of a thin Ag_2O layer therefore it has the strongest peak intensity while the other Ag_2O were too weak to be detected. Furthermore, this layer formation can be explained by the expansion of the plasma plume while it is cooled, confined, and quenched by the surrounding liquid. At extremely high temperatures the ablated species cause the ionization and vaporization of the surrounding water thereby forming a plasma-liquid interface. This results in the conversion of water into molecular and atomic components. Furthermore, this results in the formation of a cavitation bubble that rapidly expands within the liquid medium. Consequently, due to the supersaturation state of the hot plasma, GO and water species along with the confinement of the liquid medium ionic seeds of a few atoms are formed on the GO sheets which further grow to form the nanoparticles. However, during the expansion of the cavitation bubble, the concentration of the plasma and liquid species rapidly decreases while the concentration of the nanoparticles is maximized. Therefore, at elevated temperatures, the right conditions are established for the formation of Ag_2O nanoparticles [80].

4.1.4 SEM of GO, GO-AgMC, and GO-AgNS

The formation of GO, AgNPs, and GO-Ag composites was further supported by SEM micrograph. As depicted in **Figure 4.4 (a)** a typical sheet-like structure with wrinkles and folds was visible for GO. These are characteristic of the two-dimensional nature of GO. The estimated lateral size was of GO was 26.3 µm thus making it suitable for the deposition of silver ions. Therefore, the high surface area and aspect ratio make GO the optimal substrate for the anchoring of AgNPs and the formation of GO-Ag composites.

Delamination of GO flakes is observed in the composites due to the prolonged sonication of the GO solution. However, a uniform distribution of AgNPs is evident therefore indicating a large number of reactive sites present on and within GO layers. Additionally, the average size of GO-AgMC, **Figure 4.4 (b)** and GO-AgNS, **Figure 4.4 (c)** was estimated to be, 1.39 µm and 32.4 nm by ImageJ software. The difference in shape and size of these composites are crucial for their applications. Moreover, smaller clusters and spherical nanoparticles are observed in the GO-AgMC with an average size of. Therefore, the GO-AgMC is a mixture of cubic and spherical composite.

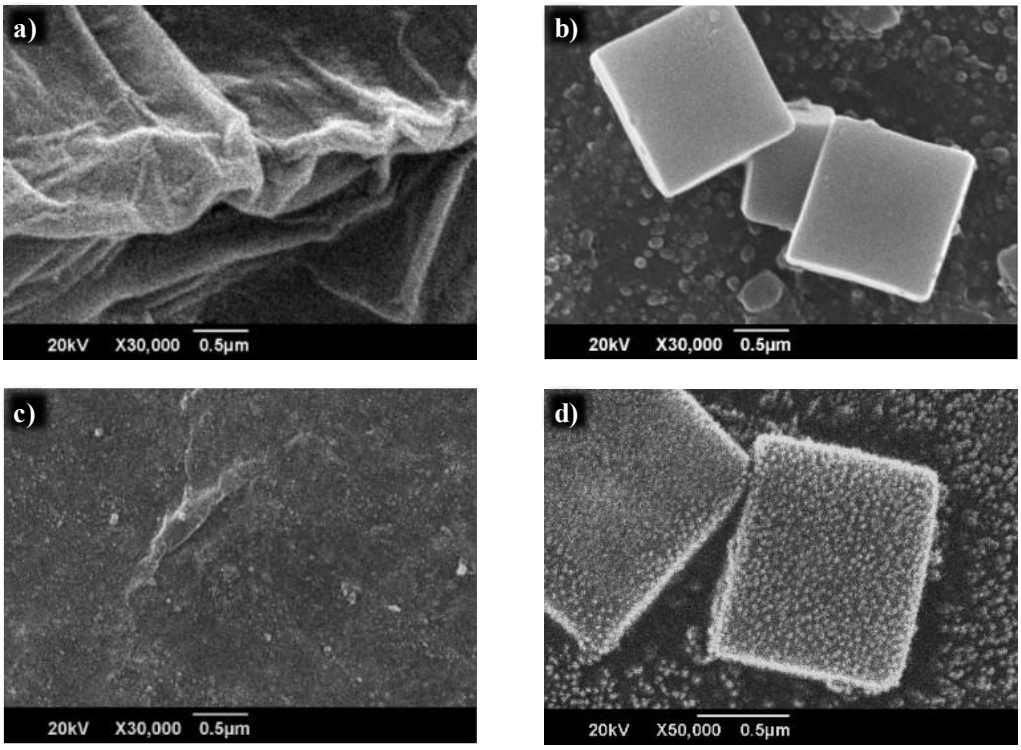

Figure 4.4: SEM images of (a) GO, (b) GO-AgMC, (c) GO-AgNS, (d) GO-AgMC after 3 months.

To check the prolonged stability of the synthesized GO-AgMC sample, an SEM spectrum was taken after three months. The sample was sonicated for 10 minutes, to redisperse the aggregated colloidal composite. As portrayed in **Figure 4.4 (d)** the GO-AgMC retained its shape and structural integrity however some small particles were deposited onto the surface. Whereas, the size of GO-AgNS increased along with the

uniform accumulation of small particles on the surface of the composite. Hence suggesting that a minor alteration in the surface morphology is caused over time due to the presence of unanchored AgNPs. Nonetheless, it could not yet be concluded if this was caused by losing their stability over time or by sonication of the sample. This is crucial for further studies as the stability of the composite is necessary for the preservation of applications based on unique properties.

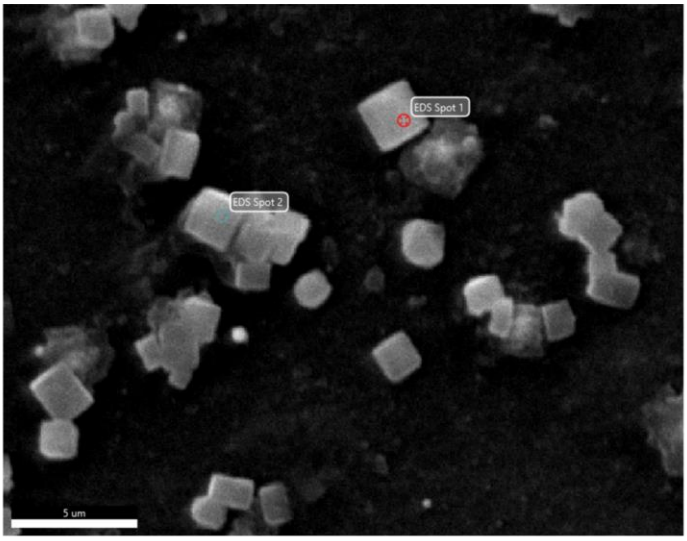

Element	Weight %	MDL	Atomic %	Error %
| New Sample | Vania 5.8 | EDS Spot 1				
C	29.5	1.38	36.5	12.4
O	67.8	0.70	63.1	10.3
A g	**2.8**	**0.90**	**0.4**	**3.2**
| New Sample | Vania 5.8 | EDS Spot 2				
C	31.6	1.30	39.0	12.0
O	65.4	0.69	60.5	10.4
A g	**3.0**	**0.75**	**0.4**	**2.7**

Figure 4.5: EDS of GO-AgMC.

As represented in **Figure 4.5** Energy Dispersive Spectroscopy (EDS) revealed distinctive elemental composition of GO-AgMC. From a specific area, the EDS analysis confirmed the detection of carbon (C), oxygen (O), and silver (Ag) with a weight

percentage of 29.5 wt%, 67.8 wt%, and 2.8 wt%, respectively. Thereby confirming the formation of GO-Ag composite with high purity. In addition, **Figure 4.6** illustrates the elemental mapping of GO-AgMC distributed over the GO sheet. The oxygen content is notably low on the surface of cubic particles thus it can be deduced the Ag_2O layer is formed in the spherical particles present in the sample instead of the more stable cubic particles.

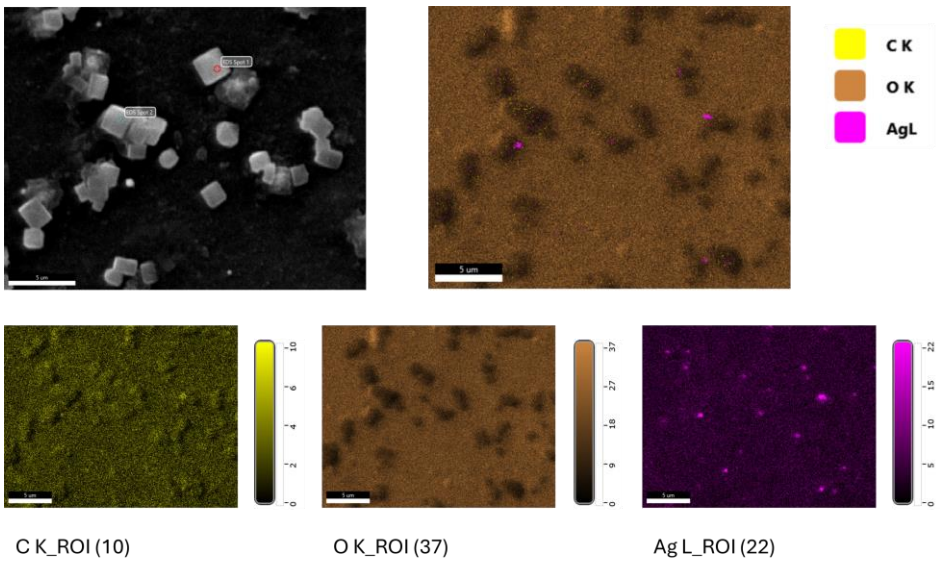

Figure 4.6: Elemental mapping of GO-AgMC.

4.1.5 Raman of GO, GO-AgMC, and GO-AgNS

Graphene oxide-based composites have a unique fingerprint region with characteristic D band and G band between 1000 cm^{-1} and 1800 cm^{-1}. Therefore, Raman analysis was performed to investigate the variations in the vibrational mode of GO after the formation of GO-Ag composites. The results, as plotted in **Figure 4.7** show GO exhibited distinctive peaks at 1347 cm^{-1} for the D band and at 1578 cm^{-1} for the G bands. With an I_D/I_G ratio of 0.85 which is consistent with already reported literature. Indicating a less defective and more ordered structure of GO. Upon the formation of composites for GO-AgMC, D peaks and G peak are observed at 1354 cm^{-1} and 1568 cm^{-1}. Thereby slightly increasing the I_D/I_G ratio to 0.86. For the GO-AgNS the D peak is at 1335 cm^{-1} and the G

peak at 1568 cm^{-1}, whereas the I_D/I_G ratio stays the same as GO; 0.85. Hence the properties of GO were preserved after the formation of composites through PLAL.

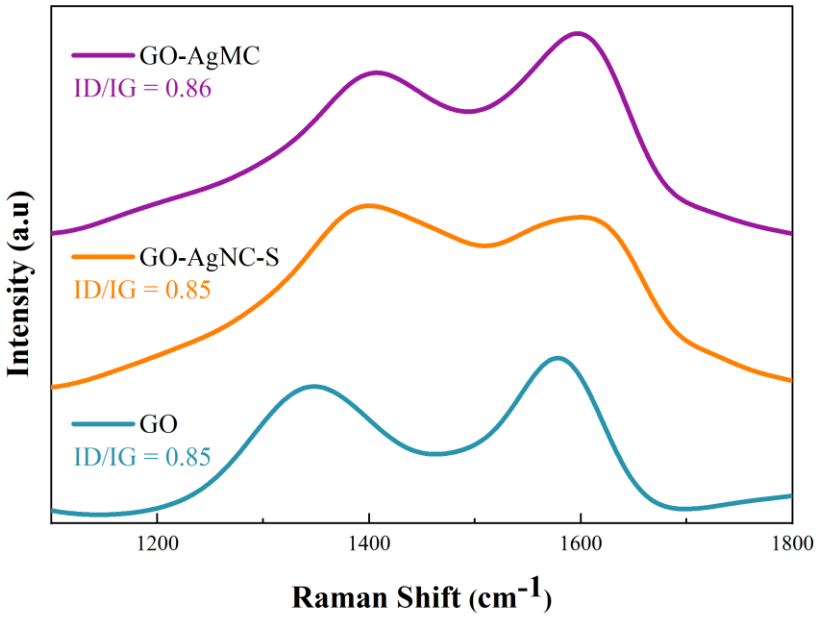

Figure 4.7: Raman spectrum of GO, GO-AgMC and GO-AgNS.

Upon depositing AgNPs the Raman signal is considerably enhanced due to the SERS effect of AgNPs [64], [81]. However, in the case of GO-AgNS, an increase in the intensity of the D band suggests the presences of added defects with a decrease in the sp^2 hybridization of the GO carbon atom. Cobos et.al. have presented a more prominent increase in the intensity of the D band upon the formation of a composite [8]. The incorporation of spherical nanoparticles within the sheets increases the defects in the sample. Thus, it can be deduced that GO-AgMC forms cubic particles adherend to the surface of GO instead of intercalating between the sheets. Owing to its micron size of GO-AgMCs. Furthermore, the increase in G band intensity suggests effective coupling of micro cubes with GO sheets hence increasing the overall charge transfer and the electronic properties of the nanocomposites. Additionally, for both samples, the peak position shift towards higher wavenumbers is attributed to the interaction of deposited AgNPs and GO hence, confirming the formation of composites.

4.1.6 Zeta Potential

GO Sonication Time	Zeta Potential
30 min	- 46.52 mV
1 hour 30 min	- 44.88 mV
2 hours	- 45.74 mV
3 hours	- 37.32 mV

Table 4-1: Zeta potential of GO during prolong sonication.

The effect of prolonged sonication on the density of the surface charge of GO was estimated through zeta potential. As listed in table 4-1 upon increasing the sonication time the zeta value shifted to a less negative value from -46 mV to -37 mV. Thereby decreasing the lateral dimensions and oxygen-containing groups of GO. However, the shift isn't significant therefore it can be deduced GO was not reduced into rGO. This is further evident from the UV-Vis analysis, Raman, and XRD.

Material	Zeta Potential
Graphene Oxide	- 37.32 mV
GO-AgMC	- 36.57 mV
GO-AgNS	- 30.05 mV

Table 4-2: Zeta potential of colloidal synthesised materials.

Subsequently, upon formation of the composite, further shift is observed in zeta values Table 4-2 which indicate a significant alteration in the surface charge density of the material. The composites have a value of -36 mV for cubic structure and -30 mV for

spherical. All the values are above the -30 mV stability benchmark used for the colloidal system.

4.2 Structure turnability/ parameter optimization of cubic composite

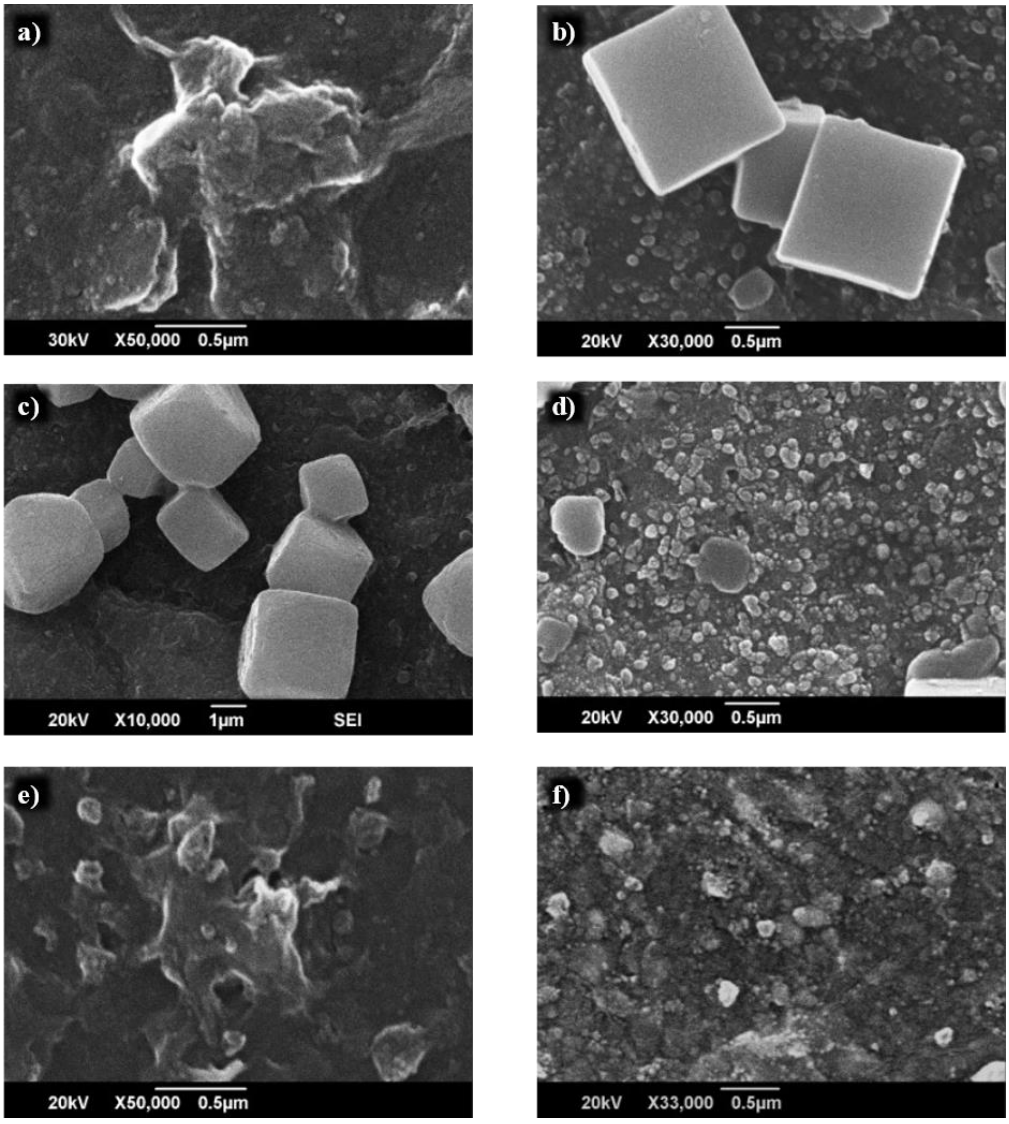

Figure 4.8: SEM image of GO-AgMC at varying parameters; (a) 5 mins, (b) 10 mins and 140 mJ, (c) 12 mins, (d) 15 mins, (e) 106 mJ, and (f) 172 mJ.

Figure 4.8 displays the change in GO-AgMC size, thereby changing the density of silver content with the variation in laser ablation time and pulsed laser energy. Initially,

time is varied from 5-15 minutes while keeping the laser energy, 140 mJ, constant. No significant AgNP peak is observed at 5 mins thus the silver content deposited on the graphene oxide isn't sufficient to form cubic nanoparticles. As illustrated in the SEM spectra of **Figure 4.8 (a)** and UV-Vis spectra in **Figure 4.9 (a)**. By increasing the time to 7 min, the cubic nanocomposite is synthesized while the respective UV-Vis spectrum reveals an AgNPs peak at 398 nm. However, it has a notably lower intensity than that of the GO present in the composite sample. As the time is further increased to 10 mins prominent sharp-edged cubic micro composite is formed with an average size of be 1.39 μm **(Figure 4.8 (b))**. The UV-Vis spectrum shows an AgNPs LSPR peak, having a similar absorption intensity to that of GO, at 404 nm.

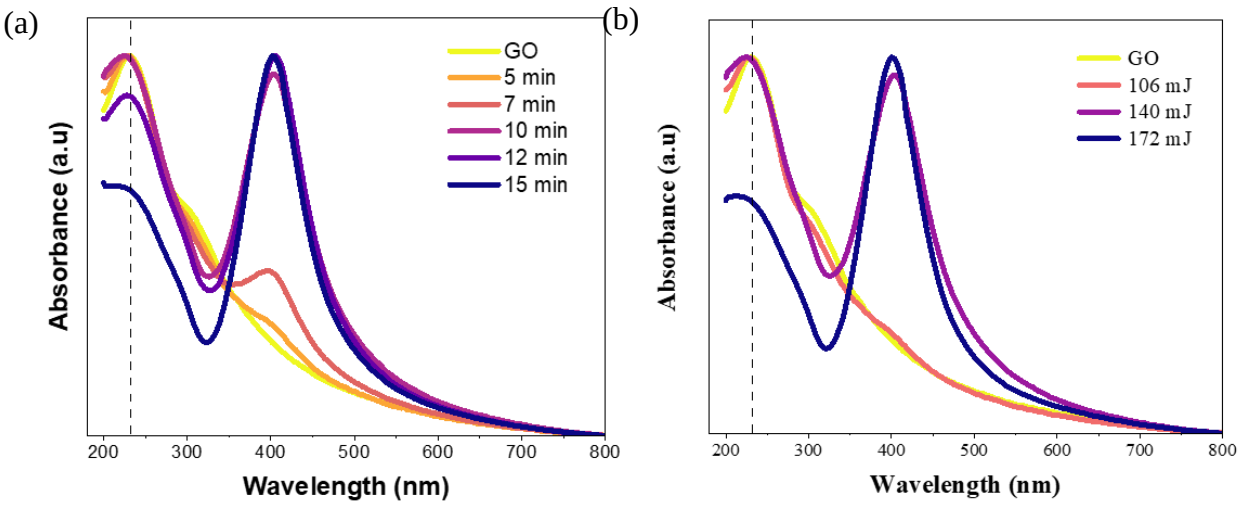

Figure 4.9: UV-Vis spectrum of GO-AgMC at (A) varying time and (B) varying energy.

Upon further increasing the time it can be observed that the cubic micro-composite grows in size with additional deposition of AgNPs however the sharp edges are lost **(Figure 4.8 (c))**. As the time is increased to 15 minutes the cubic structures interact with the laser, causing fragmentation thus clusters of particles, without any fixed morphologies are formed **(Figure 4.8 (d))**. While the peak intensity in the UV-Vis graph exceeds that of the GO. Therefore 10 mins was chosen as the ideal time for the formation of cubic

nanostructures. Consistent with previously reported study 1:1 of GO: Ag yields the most efficient results [17].

Subsequently, time was kept constant at 10 mins to vary the pulse laser energy from 106 mJ to 172 mJ. It was observed at 106 mJ that no absorption peak was detected in the UV-Vis graph, **Figure 4.9 (b)**, nor any nanoparticles were visible in the SEM spectra. Whereas at 140 mJ perfectly sharped edged microcubes were seen in the SEM spectra **(Figure 4.8 (e))** and their UV-VIS intensity matched the intensity of GO in the sample. Upon increasing the laser energy to 172 mJ a random cluster or fragmented particles was observed in the composites SEM spectra **(Figure 4.8 (f))** while the UV-Vis peak intensity exceeded the GO intensity. Therefore, prolonged ablation time and high laser energy should be avoided for the synthesis of GO-AgMC.

4.3 ANTIBACTERIAL

The antibacterial assay of the synthesized composite was carried out against gram-negative (E. coli) and gram-positive (S. aureus) through the Plate Count Method and the 96-well plate method of determining minimum inhibition concentration (MIC). For accurate determination of the bacterial growth, the OD_{600} was measured using a microplate reader.

4.3.1 GO pH-dependant antibacterial

Graphene oxide has contradicting antibacterial activity. Some report it to be an excellent antibacterial agent with strong dose-dependent cytotoxicity toward both gram-positive and gram-negative bacteria [82]. While others have reported it to increase the bacterial growth (__). Whereas Barbolina *et al*. reported GO antibacterial activity depends on its acidic impurities [32]. While the lateral size, concentration and incubation time does not affect the overall susceptibility. Similarly, Montes-Duarte *et al*. argued that the activity of GO was suppressed by the growth medium [83]. To confirm the antibacterial activity of the produced, GO the following tests were performed.

A. Plate Count Method

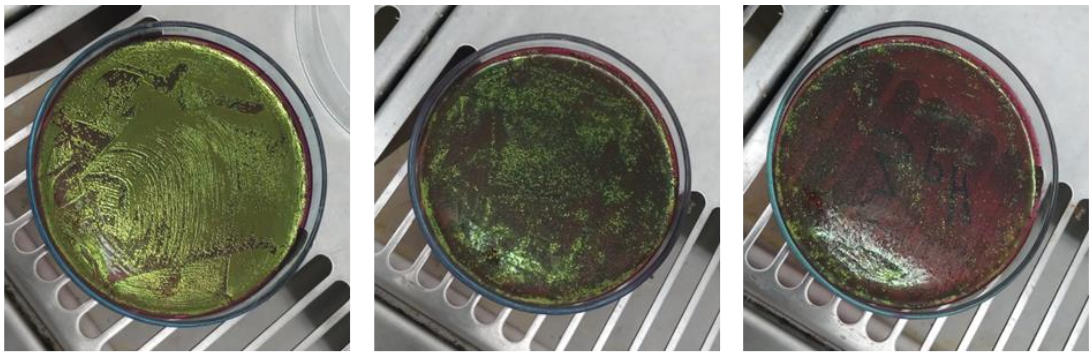

Figure 4.10: Antibacterial activity of GO produced at pH 3, 4 and 5.5 against *E. coli*.

GO was reproduced using Improved Hummers' Method and during the washup three different pH of GO were obtained. The pH of 3, 4 and 5.5 of GO powder sample was incubated with *E. coli* in the LB broth. The sample were left in a shaking incubator overnight and 50 µL of the inoculum was spread on the agar plate to evaluate the bacterial growth. As depicted in **Figure 4.10,** at completely neutral pH; 5.5, GO showed no antibacterial activity. With the plate being completely covered by bacterial growth. At pH of 4 GO did exhibit some antibacterial activity. However, it still had sufficient bacterial growth. Whereas at pH of 3, a prominent antibacterial activity of GO was observed though it wasn't capable of completely inhibiting the growth owing to the low concentration of GO used and highly concentrated bacterial inoculum. These results confirmed the finding reported by Barbolina *et al*.

B. 96 well plate test

To have a more quantitative and structured test the pH dependent antibacterial activity of GO was confirmed using the 96-well plate test. Initially synthesized GO of pH 5.5 was used by altering its pH to different pHs. Ascorbic acid was used to obtain acidic pH of 3 and 4. While Sodium Bicarbonate was used to obtain basic pH of 7 and 8. As shown in

Figure 4.**11 (a),** ascorbic acid and $NaHCO_3$ themselves didn't have an antibacterial activity therefore the obtained results were that of GO itself. As shown in the 96-well plate in the case of pH 3 GO had first 3 clear wells, hence complete inhibition of the bacteria was observed. While in the case of pH of 4 only the first 2 wells were clear. Similarly in the case of pH of 5.5, 7, and 8, the wells showed prominent bacterial growth with a visible butter-like structure being present.

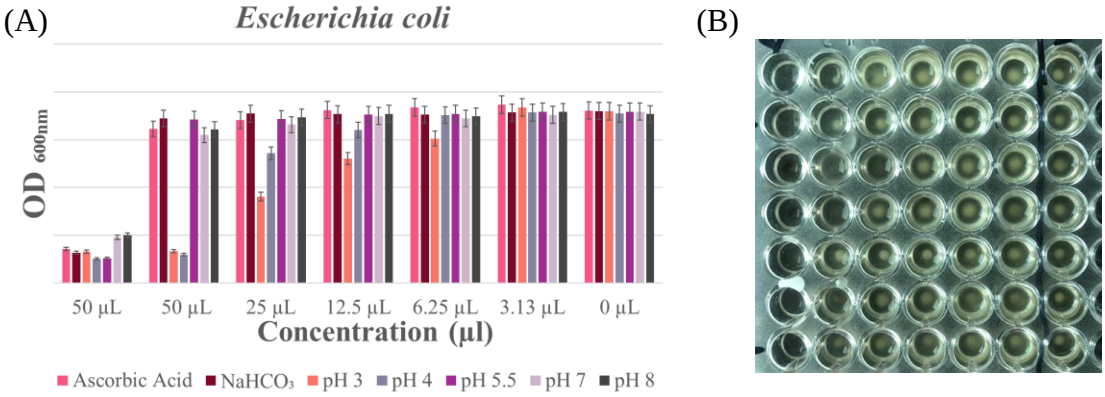

Figure 4.11: Antibacterial activity of GO at pH 3, 4, 5.5, 7 and 8 against *E. coli.*

Hence it was confirmed that GO at pH 3 exhibited proper inhibition of bacteria. The microplate photometer was used to obtain the quantitative MIC values of all the samples as illustrated in **Figure 4.11 (b)**. The GO of pH of 3 displayed a MIC value of 50 µL while pH of 4 still had some bacterial growth which was displayed in the microplate reading. Consequently, this experiment confirmed that the antibacterial activity is dependent on the pH of GO. Since it has been hypothesized that at lower pH GO have an increased ROS generation which are crucial for the antibacterial susceptibility.

4.3.2 Composites' shape-dependent antibacterial

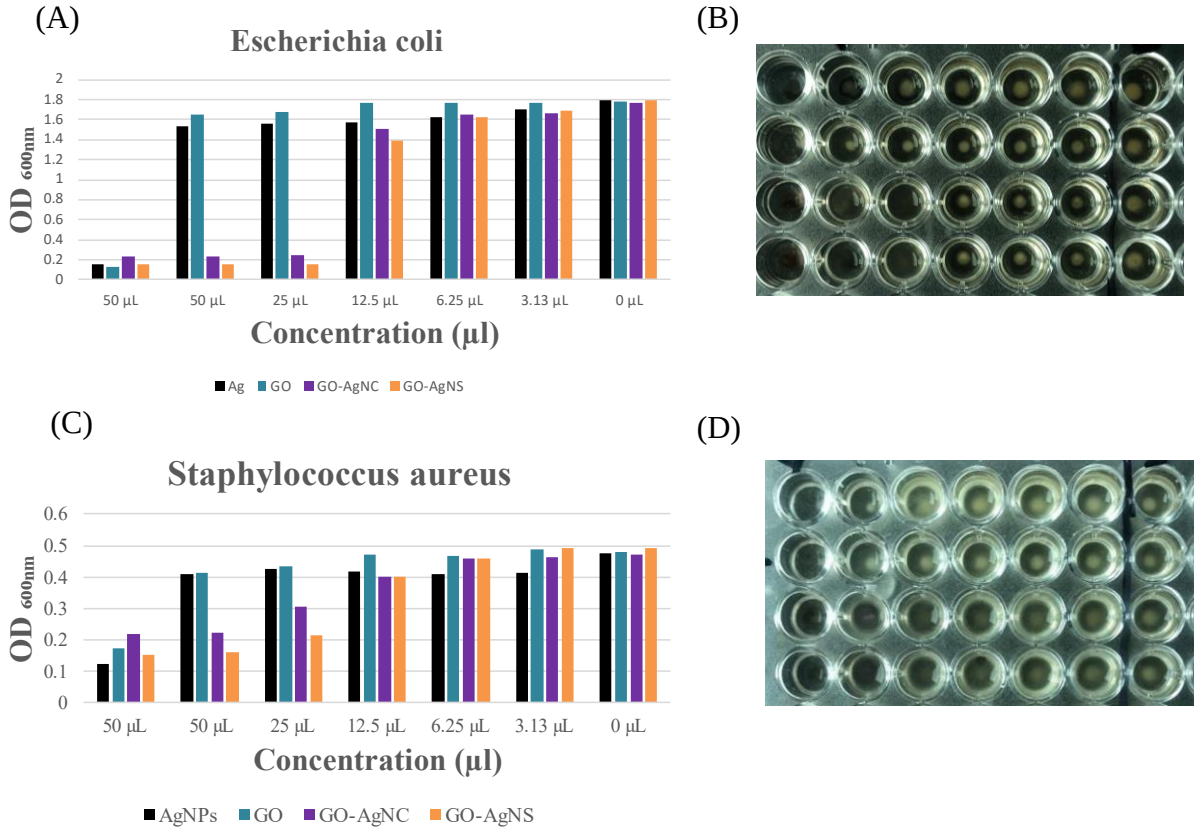

Figure 4.12: Antibacterial activity of synthesized material and the images of the 96 well plate against (A),(B) E.coli and (C), (D) S. aureus, respectively.

Under the same synthesis parameters, two different shapes and sizes of composites were formed. Spherical nanocomposite with a mean size of 32.4 nm had a similar antibacterial activity as the cubic micro-composite with an average of 1.39 µm. By varying the time of ablation and pulse laser energy, the size of the synthesized cubic nanocomposite can be varied from nano to micrometer. Previous studies have shown GO: Ag of 1:1 has the strongest antibacterial activity [17]. Since a lower ratio of Ag content isn't sufficient and higher ratios can lead to aggregation of the composites thereby decreasing the active sites and thus the antibacterial activity. Through the help of UV-visible spectrum at a 1:1 GO-AgMC perfect cubes are formed with sharp edges and uniform dispersion on the surface of the GO. Therefore, for this study laser energy of 140 mJ and laser ablation time

of 10 mins was set as the optimum synthesis parameters. Following that GO-AgNS were synthesized with the same laser parameters, in different DI water.

As demonstrated in **Figure 4.12** both composites have a similar and superior activity against E. coli and S. aureus, than that of AgNPs and GO. At such low concentrations, no activity was observed against both strains for GO and AgNPs. All of the wells had prominent turbidity and increased OD values. For AgNS and GO-AgMC no butter-like structure or turbidity was observed in the first three well against E. coli. Furthermore, through the OD reading it was confirmed that for complete inhibition of E. coli 25 μL of the synthesized composites was sufficient. In the case of S. aureus, only the first 2 wells were clear of any turbidity. The microplate reading confirmed that 50 μL of the GO-AgNS and GO-AgMC completely inhibited bacterial growth. Therefore 25 μL and 50 μL were determined to be the MIC values of both composites against E. coli and S. aureus, respectively. This agrees with several previously reported results, that state GO-Ag composites have better antibacterial susceptibility against E. coli instead of S. aureus.

AgNPs have been reported to have a size-dependent antibacterial property, with smaller spherical nanoparticles having a superior susceptibility due to the ion release mechanism and penetration of bacterial cells [84]. However, Holubnycha et al. reported bigger cubic AgNPs have five times higher susceptibility due to increased Ag^{+} ion release [85]. Similarly, this study demonstrated that the composite in the form of a micro-cubic shape had similar antibacterial activity to that of the nano-spherical shape against both E. coli and S. aureus. Since GO-AgMC exhibited a higher ion release than that of the GO-AgNS. Therefore, it can be deduced that the underlying mechanism of antibacterial activity is dependent on ion release, generation of ROS species, and oxidative stress instead of mostly depending on the penetration of cell wall by small-size spherical nanoparticles. Furthermore, strong anchoring of AgNPs on GO prevents them from being leached off from GO upon interaction with bacterial cells.

4.4 SURFACE ENHANCED RAMAN SPECTROSCOPY (SERS)

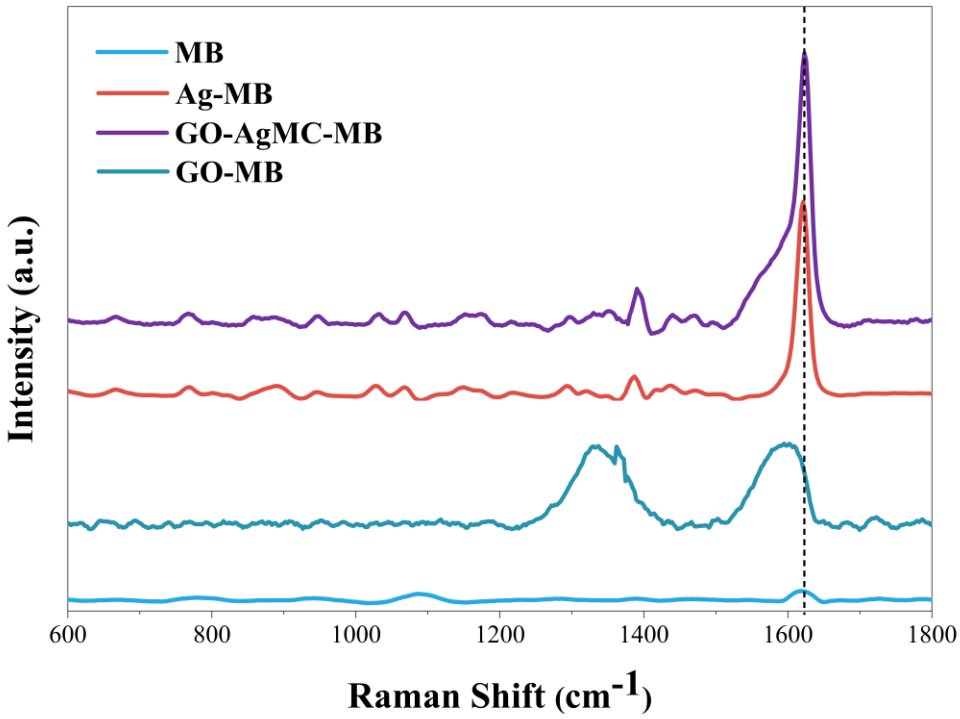

Figure 4.13: SERS of methylene blue (MB) with GO, AgNPs, and GO-AgMC.

The SERS capability of the GO, AgNP and GO- AgMC was verified by performing Raman of 1 µM Methylene Blue (MB) with and without the deposition of the samples on the substrate. Figure 4.11 shows the Raman signal of GO-MB AgNP-MB, GO-AgMC-MB and pure MB. It was observed from the Raman spectrum that the composite GO-AgMC-MB showed the highest enhancement followed by AgNP-MB. However, GO-MB did not show any significant enhancement.

The reason for the large enhancement factor for the case of GO-AgMC-MB is proposed to be because of the synergistic effect between graphene oxide and silver nanoparticles. The combination of graphene oxide and silver nanoparticles provides both electromagnetic enhancement (via silver nanoparticles) and chemical enhancement (via graphene oxide). The strong plasmonic fields that the silver nanoparticles produce is the

source of electromagnetic amplification. Additionally, the incorporated graphene oxide works as a substrate, not only stabilizing the nanoparticles but also increasing the adsorption of MB due to its large surface area and π-conjugated structure. Moreover, the presence of graphene oxide stimulates the formation of more "hot spots," i.e. areas where the electromagnetic field is intensely localized, further amplifying the Raman signal. Therefore, the composite sample can be used to detect chemical pollutants present in the environment because of the significant enhancement it can provide in the Raman spectrum.

CONCLUSIONS AND FUTURE PROSPECTIVE

Two main aims of this thesis were, 1) to investigate how the shape, size, and stability of graphene oxide-silver composite synthesized by pulsed laser ablation in liquid is effected by varying laser parameters to check. 2) The antibacterial activity against pathogenic bacteria and their capabilities of detecting organic dyes using surface-enhanced Raman spectroscopy. Regarding the effect of laser parameters, it was observed that it is possible to improve the properties of GO-Ag composites by accurately tuning different laser parameters. In particular, by using optimum laser energy and time of ablation perfectly cubic composites with enhanced activities can successfully be synthesized. It is important to note that a further increase of laser energy or too high ablation time can result in the fragmentation of the already synthesized composites into irregular shapes and sizes. Furthermore, an increase in silver concentration causes a decrease in the stability of the colloidal solution thus resulting in aggregation. However, under optimum conditions, the synthesized composites demonstrate high structural stability over a long course of time.

Additionally, it was evident by several characterization techniques that improved method results in exceptional quality and high yield of GO while PLAL forms clean, contamination-free, pure composites with uniform distribution on the GO sheets. It was possible to achieve and interpret these results due to the in-depth understanding of the fundamental mechanisms involved in the laser ablation in liquid technique and due to the insight into how each laser parameter affects the productivity of synthesized nanoparticles. Therefore, we can conclude that we succeeded in evaluating the impact of laser parameters on the size, shape, and colloidal stability of GO-Ag composites synthesized by the pulsed laser ablation technique. However, further studies are required to investigate the role of other parameters that significantly affect the productivity and properties of the composites.

The second part of this thesis aimed to investigate the antimicrobial assay of GO-Ag composites and their components against two pathogenic bacteria that are the cause of various human infections. The conducted experiment verified the effectiveness of GO as an antibacterial agent is highly dependent on the acid functionalization thereby the purity

of the exfoliated process. Moreover, the shape and concentration of the composites affect the antibacterial activity while exhibiting a better result than the individual components, GO and Ag. Likewise, the synthesized cubic composites demonstrated improved dye detection capabilities than GO and AgNPs. Hence the multifunctional composites offer an eco-friendly and feasible solution to address the increasing environmental concerns.

The current findings can further be improved by exploring the effect of other synthesis parameters on the formed materials. Such as the impact of temperature, reaction time, and washup during the exfoliation of GO. Or by changing laser parameters in different liquid mediums; alcohols, organic solvents, and in the presence of ions and surfactants. In addition, the antibacterial and SERS effects of varying sizes of cubic composites could be investigated. Similarly, catalytical activity, water purification efficiency, antifouling properties, integration into coatings, and long-term stability under different environmental conditions could be explored. Lastly, before fully integrating the proposed composite in various environmental applications it is essential to know the cytotoxicity, ecological safety, and degradation behavior of GO-Ag nanocomposites.

REFERENCES

[1] S. Sharma, S. Tiwari, A. Hasan, V. Saxena, and L. M. Pandey, "Recent advances in conventional and contemporary methods for remediation of heavy metal-contaminated soils," *3 Biotech*, vol. 8, no. 4, p. 216, Apr. 2018, doi: 10.1007/s13205-018-1237-8.

[2] K. H. Vardhan, P. S. Kumar, and R. C. Panda, "A review on heavy metal pollution, toxicity and remedial measures: Current trends and future perspectives," *J Mol Liq*, vol. 290, p. 111197, Sep. 2019, doi: 10.1016/j.molliq.2019.111197.

[3] E. Bahcelioglu, D. Doganay, S. Coskun, H. E. Unalan, and T. H. Erguder, "A Point-of-Use (POU) Water Disinfection: Silver Nanowire Decorated Glass Fiber Filters," *Journal of Water Process Engineering*, vol. 38, p. 101616, Dec. 2020, doi: 10.1016/j.jwpe.2020.101616.

[4] M. S. Morehead and C. Scarbrough, "Emergence of Global Antibiotic Resistance," *Primary Care: Clinics in Office Practice*, vol. 45, no. 3, pp. 467–484, Sep. 2018, doi: 10.1016/j.pop.2018.05.006.

[5] Y. Zhu *et al.*, "Graphene and Graphene Oxide: Synthesis, Properties, and Applications," *Advanced Materials*, vol. 22, no. 35, pp. 3906–3924, Sep. 2010, doi: 10.1002/adma.201001068.

[6] A. M. Pinto, I. C. Gonçalves, and F. D. Magalhães, "Graphene-based materials biocompatibility: A review," *Colloids Surf B Biointerfaces*, vol. 111, pp. 188–202, Nov. 2013, doi: 10.1016/j.colsurfb.2013.05.022.

[7] A. Jiříčková, O. Jankovský, Z. Sofer, and D. Sedmidubský, "Synthesis and Applications of Graphene Oxide," *Materials*, vol. 15, no. 3, p. 920, Jan. 2022, doi: 10.3390/ma15030920.

[8] M. Cobos, I. De-La-Pinta, G. Quindós, M. J. Fernández, and M. D. Fernández, "Graphene Oxide–Silver Nanoparticle Nanohybrids: Synthesis, Characterization, and Antimicrobial Properties," *Nanomaterials*, vol. 10, no. 2, p. 376, Feb. 2020, doi: 10.3390/nano10020376.

[9] E. F. Joel and G. Lujanienė, "Progress in Graphene Oxide Hybrids for Environmental Applications," *Environments*, vol. 9, no. 12, p. 153, Dec. 2022, doi: 10.3390/environments9120153.

[10] K. Thakur and B. Kandasubramanian, "Graphene and Graphene Oxide-Based Composites for Removal of Organic Pollutants: A Review," *J Chem Eng Data*, vol. 64, no. 3, pp. 833–867, Mar. 2019, doi: 10.1021/acs.jced.8b01057.

[11] S. Singh *et al.*, “Novel insights into graphene oxide-based adsorbents for remediation of hazardous pollutants from aqueous solutions: A comprehensive review,” *J Mol Liq*, vol. 369, p. 120821, Jan. 2023, doi: 10.1016/j.molliq.2022.120821.

[12] N. C. Joshi and P. Gururani, “Advances of graphene oxide based nanocomposite materials in the treatment of wastewater containing heavy metal ions and dyes,” *Current Research in Green and Sustainable Chemistry*, vol. 5, p. 100306, 2022, doi: 10.1016/j.crgsc.2022.100306.

[13] H. Bai *et al.*, “Insight into the Mechanism of Graphene Oxide Degradation via the Photo-Fenton Reaction,” *The Journal of Physical Chemistry C*, vol. 118, no. 19, pp. 10519–10529, May 2014, doi: 10.1021/jp503413s.

[14] S. Hazra and S. Basu, “Graphene-Oxide Nano Composites for Chemical Sensor Applications,” *C (Basel)*, vol. 2, no. 2, p. 12, Apr. 2016, doi: 10.3390/c2020012.

[15] X.-G. Gao, L.-X. Cheng, W.-S. Jiang, X.-K. Li, and F. Xing, “Graphene and its Derivatives-Based Optical Sensors,” *Front Chem*, vol. 9, Feb. 2021, doi: 10.3389/fchem.2021.615164.

[16] X. Zou, L. Zhang, Z. Wang, and Y. Luo, “Mechanisms of the Antimicrobial Activities of Graphene Materials,” *J Am Chem Soc*, vol. 138, no. 7, pp. 2064–2077, Mar. 2016, doi: 10.1021/jacs.5b11411.

[17] J. Tang *et al.*, “Graphene Oxide–Silver Nanocomposite As a Highly Effective Antibacterial Agent with Species-Specific Mechanisms,” *ACS Appl Mater Interfaces*, vol. 5, no. 9, pp. 3867–3874, May 2013, doi: 10.1021/am4005495.

[18] Z. Xiu, Q. Zhang, H. L. Puppala, V. L. Colvin, and P. J. J. Alvarez, “Negligible Particle-Specific Antibacterial Activity of Silver Nanoparticles,” *Nano Lett*, vol. 12, no. 8, pp. 4271–4275, Aug. 2012, doi: 10.1021/nl301934w.

[19] P. Nancy *et al.*, “Fabrication of Silver-Decorated Graphene Oxide Nanohybrids via Pulsed Laser Ablation with Excellent Antimicrobial and Optical Limiting Performance,” *Nanomaterials*, vol. 11, no. 4, p. 880, Mar. 2021, doi: 10.3390/nano11040880.

[20] A. A. Menazea and M. K. Ahmed, “Silver and copper oxide nanoparticles-decorated graphene oxide via pulsed laser ablation technique: Preparation, characterization, and photoactivated antibacterial activity,” *Nano-Structures & Nano-Objects*, vol. 22, p. 100464, Apr. 2020, doi: 10.1016/j.nanoso.2020.100464.

[21] A. Rana and A. S. Parmar, “Re-exploring silver nanoparticles and its potential applications,” *Nanotechnology for Environmental Engineering*, vol. 8, no. 3, pp. 789–804, Sep. 2023, doi: 10.1007/s41204-022-00301-w.

[22] L. Zhang, P. Chen, Y. Xu, W. Nie, and Y. Zhou, “Enhanced photo-induced antibacterial application of graphene oxide modified by sodium anthraquinone-2-sulfonate under visible light,” *Appl Catal B*, vol. 265, p. 118572, May 2020, doi: 10.1016/j.apcatb.2019.118572.

[23] S. Zhao, Z. Zhao, Z. Yang, L. Ke, S. Kitipornchai, and J. Yang, “Functionally graded graphene reinforced composite structures: A review,” *Eng Struct*, vol. 210, p. 110339, May 2020, doi: 10.1016/j.engstruct.2020.110339.

[24] A. Sasidharan *et al.*, “Differential nano-bio interactions and toxicity effects of pristine versus functionalized graphene,” *Nanoscale*, vol. 3, no. 6, p. 2461, 2011, doi: 10.1039/c1nr10172b.

[25] Z. Sun, Z. Yan, J. Yao, E. Beitler, Y. Zhu, and J. M. Tour, “Growth of graphene from solid carbon sources,” *Nature*, vol. 468, no. 7323, pp. 549–552, Nov. 2010, doi: 10.1038/nature09579.

[26] B. C. Brodie, “On the Atomic Weight of Graphite,” 1859. [Online]. Available: https://about.jstor.org/terms

[27] L. Staudenmaier, “Verfahren zur Darstellung der Graphitsäure,” *Berichte der deutschen chemischen Gesellschaft*, vol. 31, no. 2, pp. 1481–1487, May 1898, doi: 10.1002/cber.18980310237.

[28] W. S. Hummers and R. E. Offeman, “Preparation of Graphitic Oxide,” *J Am Chem Soc*, vol. 80, no. 6, pp. 1339–1339, Mar. 1958, doi: 10.1021/ja01539a017.

[29] T. Chen *et al.*, “High throughput exfoliation of graphene oxide from expanded graphite with assistance of strong oxidant in modified Hummers method,” *J Phys Conf Ser*, vol. 188, p. 012051, Sep. 2009, doi: 10.1088/1742-6596/188/1/012051.

[30] D. C. Marcano *et al.*, “Improved synthesis of graphene oxide,” *ACS Nano*, vol. 4, no. 8, pp. 4806–4814, Aug. 2010, doi: 10.1021/nn1006368.

[31] J. Chen, B. Yao, C. Li, and G. Shi, “An improved Hummers method for eco-friendly synthesis of graphene oxide,” *Carbon N Y*, vol. 64, pp. 225–229, Nov. 2013, doi: 10.1016/j.carbon.2013.07.055.

[32] I. Barbolina, C. R. Woods, N. Lozano, K. Kostarelos, K. S. Novoselov, and I. S. Roberts, “Purity of graphene oxide determines its antibacterial activity,” *2d Mater*, vol. 3, no. 2, May 2016, doi: 10.1088/2053-1583/3/2/025025.

[33] R. Al-Gaashani, Y. Zakaria, O. S. Lee, J. Ponraj, V. Kochkodan, and M. A. Atieh, “Effects of preparation temperature on production of graphene oxide by novel chemical processing,” *Ceram Int*, vol. 47, no. 7, pp. 10113–10122, Apr. 2021, doi: 10.1016/j.ceramint.2020.12.159.

[34] T. Tene, M. Guevara, F. Benalcázar Palacios, T. P. Morocho Barrionuevo, C. Vacacela Gomez, and S. Bellucci, "Optical properties of graphene oxide," *Front Chem*, vol. 11, 2023, doi: 10.3389/fchem.2023.1214072.

[35] Y. Tian, Z. Yu, L. Cao, X. L. Zhang, C. Sun, and D.-W. Wang, "Graphene oxide: An emerging electromaterial for energy storage and conversion," *Journal of Energy Chemistry*, vol. 55, pp. 323–344, Apr. 2021, doi: 10.1016/j.jechem.2020.07.006.

[36] L. Dong, R. R. S. Gari, Z. Li, M. M. Craig, and S. Hou, "Graphene-supported platinum and platinum–ruthenium nanoparticles with high electrocatalytic activity for methanol and ethanol oxidation," *Carbon N Y*, vol. 48, no. 3, pp. 781–787, Mar. 2010, doi: 10.1016/j.carbon.2009.10.027.

[37] R. B. Rakhi, W. Chen, D. Cha, and H. N. Alshareef, "High performance supercapacitors using metal oxide anchored graphene nanosheet electrodes," *J Mater Chem*, vol. 21, no. 40, p. 16197, 2011, doi: 10.1039/c1jm12963e.

[38] L. Zhu *et al.*, "Graphene Oxide Composite Membranes for Water Purification," *ACS Appl Nano Mater*, vol. 5, no. 3, pp. 3643–3653, Mar. 2022, doi: 10.1021/acsanm.1c04322.

[39] S. Khaliha *et al.*, "Graphene oxide nanosheets for drinking water purification by tandem adsorption and microfiltration," *Sep Purif Technol*, vol. 300, p. 121826, Nov. 2022, doi: 10.1016/j.seppur.2022.121826.

[40] Y. Han, Z. Xu, and C. Gao, "Ultrathin Graphene Nanofiltration Membrane for Water Purification," *Adv Funct Mater*, vol. 23, no. 29, pp. 3693–3700, Aug. 2013, doi: 10.1002/adfm.201202601.

[41] D. Subara and I. Jaswir, "Gold Nanoparticles: Synthesis and application for Halal Authentication in Meat and Meat Products," *Int J Adv Sci Eng Inf Technol*, vol. 8, no. 4–2, pp. 1633–1641, Sep. 2018, doi: 10.18517/ijaseit.8.4-2.7055.

[42] H. K. Choi, M.-J. Lee, S. N. Lee, T.-H. Kim, and B.-K. Oh, "Noble Metal Nanomaterial-Based Biosensors for Electrochemical and Optical Detection of Viruses Causing Respiratory Illnesses," *Front Chem*, vol. 9, May 2021, doi: 10.3389/fchem.2021.672739.

[43] Z.-Z. J. Lim, J.-E. J. Li, C.-T. Ng, L.-Y. L. Yung, and B.-H. Bay, "Gold nanoparticles in cancer therapy," *Acta Pharmacol Sin*, vol. 32, no. 8, pp. 983–990, Aug. 2011, doi: 10.1038/aps.2011.82.

[44] F.-Y. Kong, J.-W. Zhang, R.-F. Li, Z.-X. Wang, W.-J. Wang, and W. Wang, "Unique Roles of Gold Nanoparticles in Drug Delivery, Targeting and Imaging Applications," *Molecules*, vol. 22, no. 9, p. 1445, Aug. 2017, doi: 10.3390/molecules22091445.

[45] A.-M. Alam and Y.-S. Shon, “Water-Soluble Noble Metal Nanoparticle Catalysts Capped with Small Organic Molecules for Organic Transformations in Water,” *ACS Appl Nano Mater*, vol. 4, no. 4, pp. 3294–3318, Apr. 2021, doi: 10.1021/acsanm.1c00335.

[46] M. Pan *et al.*, “Noble Metal Nanostructured Materials for Chemical and Biosensing Systems,” *Nanomaterials*, vol. 10, no. 2, p. 209, Jan. 2020, doi: 10.3390/nano10020209.

[47] Y. A. Krutyakov, A. A. Kudrinskiy, A. Y. Olenin, and G. V Lisichkin, “Synthesis and properties of silver nanoparticles: advances and prospects,” *Russian Chemical Reviews*, vol. 77, no. 3, pp. 233–257, Mar. 2008, doi: 10.1070/RC2008v077n03ABEH003751.

[48] A. Syafiuddin, Salmiati, M. R. Salim, A. Beng Hong Kueh, T. Hadibarata, and H. Nur, “A Review of Silver Nanoparticles: Research Trends, Global Consumption, Synthesis, Properties, and Future Challenges,” *Journal of the Chinese Chemical Society*, vol. 64, no. 7, pp. 732–756, Jul. 2017, doi: 10.1002/jccs.201700067.

[49] R. Vishwanath and B. Negi, “Conventional and green methods of synthesis of silver nanoparticles and their antimicrobial properties,” *Current Research in Green and Sustainable Chemistry*, vol. 4, p. 100205, 2021, doi: 10.1016/j.crgsc.2021.100205.

[50] H. Zeng *et al.*, “Nanomaterials via Laser Ablation/Irradiation in Liquid: A Review,” *Adv Funct Mater*, vol. 22, no. 7, pp. 1333–1353, Apr. 2012, doi: 10.1002/adfm.201102295.

[51] V. Amendola and M. Meneghetti, “What controls the composition and the structure of nanomaterials generated by laser ablation in liquid solution?,” *Phys. Chem. Chem. Phys.*, vol. 15, no. 9, pp. 3027–3046, 2013, doi: 10.1039/C2CP42895D.

[52] D. Zhang, B. Gökce, and S. Barcikowski, “Laser Synthesis and Processing of Colloids: Fundamentals and Applications,” *Chem Rev*, vol. 117, no. 5, pp. 3990–4103, Mar. 2017, doi: 10.1021/acs.chemrev.6b00468.

[53] D. Zhang, J. Liu, and C. Liang, “Perspective on how laser-ablated particles grow in liquids,” *Sci China Phys Mech Astron*, vol. 60, no. 7, p. 074201, Jul. 2017, doi: 10.1007/s11433-017-9035-8.

[54] T. Tsuji, K. Iryo, Y. Nishimura, and M. Tsuji, “Preparation of metal colloids by a laser ablation technique in solution: influence of laser wavelength on the ablation efficiency (II),” *J Photochem Photobiol A Chem*, vol. 145, no. 3, pp. 201–207, Dec. 2001, doi: 10.1016/S1010-6030(01)00583-4.

[55] X. Zheng *et al.*, “Laser-Induced Growth of Monodisperse Silver Nanoparticles with Tunable Surface Plasmon Resonance Properties and a Wavelength Self-Limiting Effect,” *The Journal of Physical Chemistry C*, vol. 111, no. 41, pp. 14962–14967, Oct. 2007, doi: 10.1021/jp074583b.

[56] F. Mafuné, J. Kohno, Y. Takeda, T. Kondow, and H. Sawabe, “Formation and Size Control of Silver Nanoparticles by Laser Ablation in Aqueous Solution,” *J Phys Chem B*, vol. 104, no. 39, pp. 9111–9117, Oct. 2000, doi: 10.1021/jp001336y.

[57] N. V. Tarasenko, A. V. Butsen, and E. A. Nevar, “Laser-induced modification of metal nanoparticles formed by laser ablation technique in liquids,” *Appl Surf Sci*, vol. 247, no. 1–4, pp. 418–422, Jul. 2005, doi: 10.1016/j.apsusc.2005.01.093.

[58] R. ZAMIRI, B. Z. AZMI, H. A. AHANGAR, G. ZAMIRI, M. S. HUSIN, and Z. A. WAHAB, “Preparation and characterization of silver nanoparticles in natural polymers using laser ablation,” *Bulletin of Materials Science*, vol. 35, no. 5, pp. 727–731, Oct. 2012, doi: 10.1007/s12034-012-0360-0.

[59] T. Tsuji, Y. Higashi, M. Tsuji, Y. Ishikawa, and N. Koshizaki, “Preparation of submicron-sized spherical particles of gold using laser-induced melting in liquids and low-toxic stabilizing reagent,” *Appl Surf Sci*, vol. 348, pp. 10–15, Sep. 2015, doi: 10.1016/j.apsusc.2015.02.057.

[60] A. Pyatenko, M. Yamaguchi, and M. Suzuki, “Mechanisms of Size Reduction of Colloidal Silver and Gold Nanoparticles Irradiated by Nd:YAG Laser,” *The Journal of Physical Chemistry C*, vol. 113, no. 21, pp. 9078–9085, May 2009, doi: 10.1021/jp808300q.

[61] M. Noga, J. Milan, A. Frydrych, and K. Jurowski, “Toxicological Aspects, Safety Assessment, and Green Toxicology of Silver Nanoparticles (AgNPs)—Critical Review: State of the Art,” *Int J Mol Sci*, vol. 24, no. 6, p. 5133, Mar. 2023, doi: 10.3390/ijms24065133.

[62] D. B. Thinh *et al.*, “A review of silver-dopped graphene oxide nanocomposite: Synthesis and multifunctional applications,” *Vietnam Journal of Chemistry*, vol. 60, no. 5, pp. 553–570, Oct. 2022, doi: 10.1002/vjch.202200034.

[63] W. Yang, M. Pan, C. Huang, Z. Zhao, J. Wang, and H. Zeng, “Graphene oxide-based noble-metal nanoparticles composites for environmental application,” *Composites Communications*, vol. 24, p. 100645, Apr. 2021, doi: 10.1016/j.coco.2021.100645.

[64] S. Murphy, L. Huang, and P. V. Kamat, “Reduced Graphene Oxide–Silver Nanoparticle Composite as an Active SERS Material,” *The Journal of Physical Chemistry C*, vol. 117, no. 9, pp. 4740–4747, Mar. 2013, doi: 10.1021/jp3108528.

[65] K. S. Khashan, G. M. Sulaiman, R. Mahdi, and A. kadhim, “The effect of laser energy on the properties of carbon nanotube—iron oxide nanoparticles composite prepared via pulsed laser ablation in liquid,” *Mater Res Express*, vol. 5, no. 10, p. 105004, Aug. 2018, doi: 10.1088/2053-1591/aadabc.

[66] H. He *et al.*, “Green and Tunable Decoration of Graphene with Spherical Nanoparticles Based on Laser Ablation in Water: A Case of Ag

Nanoparticle/Graphene Oxide Sheet Composites," *Langmuir*, vol. 32, no. 7, pp. 1667–1673, Feb. 2016, doi: 10.1021/acs.langmuir.5b03527.

[67] R. Al-Assaly and A. Al-Nafiey, "Synthesize rGO-Ag NPs nanocomposite by a simple physical method and applying in water treatment," 2022, p. 080030. doi: 10.1063/5.0067431.

[68] S. B. Malik *et al.*, "Synthesis and Characterization of Silver and Graphene Nanocomposites and Their Antimicrobial and Photocatalytic Potentials," *Molecules*, vol. 27, no. 16, p. 5184, Aug. 2022, doi: 10.3390/molecules27165184.

[69] T. Vi, S. Kumar, J.-H. Pang, Y.-K. Liu, D. Chen, and S. Lue, "Synergistic Antibacterial Activity of Silver-Loaded Graphene Oxide towards Staphylococcus Aureus and Escherichia Coli," *Nanomaterials*, vol. 10, no. 2, p. 366, Feb. 2020, doi: 10.3390/nano10020366.

[70] A. Lange *et al.*, "Nanocomposites of Graphene Oxide—Silver Nanoparticles for Enhanced Antibacterial Activity: Mechanism of Action and Medical Textiles Coating," *Materials*, vol. 15, no. 9, p. 3122, Apr. 2022, doi: 10.3390/ma15093122.

[71] H. Naeem, M. Ajmal, R. B. Qureshi, S. T. Muntha, M. Farooq, and M. Siddiq, "Facile synthesis of graphene oxide–silver nanocomposite for decontamination of water from multiple pollutants by adsorption, catalysis and antibacterial activity," *J Environ Manage*, vol. 230, pp. 199–211, Jan. 2019, doi: 10.1016/j.jenvman.2018.09.061.

[72] V. R. Dandu Kamakshi Gari and M. Kim, "Removal of Pb(II) using silver nanoparticles deposited graphene oxide: equilibrium and kinetic studies," *Monatshefte für Chemie - Chemical Monthly*, vol. 146, no. 9, pp. 1445–1453, Sep. 2015, doi: 10.1007/s00706-015-1429-4.

[73] C. M. Park, D. Wang, J. Han, J. Heo, and C. Su, "Evaluation of the colloidal stability and adsorption performance of reduced graphene oxide–elemental silver/magnetite nanohybrids for selected toxic heavy metals in aqueous solutions," *Appl Surf Sci*, vol. 471, pp. 8–17, Mar. 2019, doi: 10.1016/j.apsusc.2018.11.240.

[74] J. Mathew, N. John, and B. Mathew, "Graphene oxide-incorporated silver-based photocatalysts for enhanced degradation of organic toxins: a review," *Environmental Science and Pollution Research*, vol. 30, no. 7, pp. 16817–16851, Jan. 2023, doi: 10.1007/s11356-022-25026-w.

[75] S. Zhong, B. Wang, H. Zhou, C. Li, X. Peng, and S. Zhang, "Fabrication and characterization of Ag/BiOI/GO composites with enhanced photocatalytic activity," *J Alloys Compd*, vol. 806, pp. 401–409, Oct. 2019, doi: 10.1016/j.jallcom.2019.07.223.

[76] Y. Zhang, N. Li, B. Liu, and H. Zhang, “Hydrogen Peroxide and Dopamine Sensors Based on Electrodeposition of Reduced Graphene Oxide/Silver Nanoparticles,” *Sensors*, vol. 24, no. 2, p. 355, Jan. 2024, doi: 10.3390/s24020355.

[77] N. M. Dat *et al.*, “Facile Synthesis of Eco-Friendly Silver@Graphene Oxide Nanocomposite for Optical Sensing,” *ChemistrySelect*, vol. 8, no. 5, Feb. 2023, doi: 10.1002/slct.202204183.

[78] Z. Y. X. W. Maocong Hu, “Characterization techniques for graphene-based materials in catalysis,” *AIMS Mater Sci*, vol. 4, no. 3, 2017.

[79] Y. Meng, “A sustainable approach to fabricating ag nanoparticles/PVA hybrid nanofiber and its catalytic activity,” *Nanomaterials*, vol. 5, no. 2, pp. 1124–1135, Jun. 2015, doi: 10.3390/nano5021124.

[80] N. G. Semaltianos, W. Perrie, S. Romani, R. J. Potter, G. Dearden, and K. G. Watkins, “Polymer-nanoparticle composites composed of PEDOT:PSS and nanoparticles of Ag synthesised by laser ablation,” *Colloid Polym Sci*, vol. 290, no. 3, pp. 213–220, Feb. 2012, doi: 10.1007/s00396-011-2533-6.

[81] E. Giorgetti, P. Marsili, F. Giammanco, S. Trigari, C. Gellini, and M. Muniz-Miranda, “Ag nanoparticles obtained by pulsed laser ablation in water: surface properties and SERS activity,” *Journal of Raman Spectroscopy*, vol. 46, no. 5, pp. 462–469, May 2015, doi: 10.1002/jrs.4677.

[82] A. N. Ghulam, O. A. L. Dos Santos, L. Hazeem, B. P. Backx, M. Bououdina, and S. Bellucci, “Graphene Oxide (GO) Materials—Applications and Toxicity on Living Organisms and Environment,” Jun. 01, 2022, *MDPI*. doi: 10.3390/jfb13020077.

[83] G. G. Montes-Duarte *et al.*, “Key parameters to enhance the antibacterial effect of graphene oxide in solution,” *RSC Adv*, vol. 11, no. 12, pp. 6509–6516, 2021, doi: 10.1039/D0RA07945F.

[84] A. Menichetti, A. Mavridi-Printezi, D. Mordini, and M. Montalti, “Effect of Size, Shape and Surface Functionalization on the Antibacterial Activity of Silver Nanoparticles,” May 01, 2023, *MDPI*. doi: 10.3390/jfb14050244.

[85] V. Holubnycha *et al.*, “Antimicrobial Activity of Two Different Types of Silver Nanoparticles against Wide Range of Pathogenic Bacteria,” *Nanomaterials*, vol. 14, no. 2, Jan. 2024, doi: 10.3390/nano14020137.